

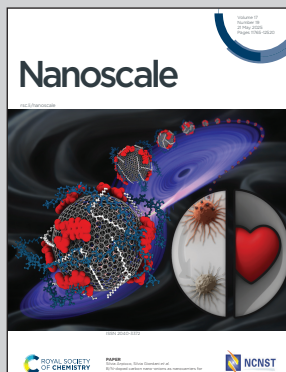
Showcasing research from Professor Dr. Sanjiv Dhingra's laboratory, St. Boniface Hospital Research Centre, Max Rady College of Medicine, University of Manitoba, Winnipeg, Canada.

MXenes in healthcare: transformative applications and challenges in medical diagnostics and therapeutics

This review highlights the exciting potential of MXenes, a new class of 2D materials in revolutionizing healthcare. It explores how these materials improve wearable sensors, support tissue repair, and help fight infections through antimicrobial and immune-modulatory properties. The review also discusses challenges like safety and large-scale production, offering solutions to help bring MXene-based technologies into real-world medical use.

Image reproduced by permission of Dr Sanjiv Dhingra from *Nanoscale*, 2025, **17**, 11785.

## As featured in:



See Sanjiv Dhingra *et al.*, *Nanoscale*, 2025, **17**, 11785.



Cite this: *Nanoscale*, 2025, **17**, 11785

## MXenes in healthcare: transformative applications and challenges in medical diagnostics and therapeutics

Keshav Narayan Alagarsamy, †<sup>a</sup> Leena Regi Saleth, †<sup>a</sup> Kateryna Diedkova, <sup>b,c</sup> Veronika Zahorodna, <sup>d</sup> Oleksiy Gogotsi, <sup>c,d</sup> Maksym Pogorielov<sup>b,c</sup> and Sanjiv Dhingra \*<sup>a</sup>

MXenes, a novel class of two-dimensional transition metal carbides, exhibit exceptional physicochemical properties that make them highly promising for biomedical applications. Their application has been explored in bioinstrumentation, tissue engineering, and infectious disease management. In bioinstrumentation, MXenes enhance the sensitivity and response time of wearable sensors, including piezoresistive, electrochemical, and electrophysiological sensors. They also function effectively as contrast agents in MRI and CT imaging for cancer diagnostics and therapy. In tissue engineering, MXenes contribute to both hard and soft tissue regeneration, playing a key role in neural, cardiac, skin and bone repair. Additionally, they offer innovative solutions in combating infectious and inflammatory diseases by facilitating antimicrobial surfaces and immune modulation. Despite their potential, several challenges hinder the clinical translation of MXene-based technologies. Issues related to synthesis, scalability, biocompatibility, and long-term safety must be addressed to ensure their practical implementation in medical applications. This review provides a comprehensive overview of MXenes in next-generation medical diagnostics, including the role they play in wearable sensors and imaging contrast agents. It further explores their applications in tissue engineering and infectious disease management, highlighting their antimicrobial and immunomodulatory properties. Finally, we discuss the key barriers to clinical translation and propose strategies for overcoming these limitations. This review aims to bridge current advancements with future opportunities for integration of MXenes in healthcare.

Received 18th November 2024,  
Accepted 1st April 2025

DOI: 10.1039/d4nr04853a  
[rsc.li/nanoscale](http://rsc.li/nanoscale)

### 1. Introduction

MXenes, a newly identified family of two-dimensional (2D) materials, are composed of transition metal carbides, nitrides, and carbonitrides.<sup>1</sup> The outstanding physicochemical properties of these materials have made them desirable candidates for various applications.<sup>2,3</sup> In the initial process of generating MXenes, the “A” element from the MAX phase is selec-

tively removed from layered carbides and nitrides, resulting in a multi-layered compound. Generally, they are represented by the standard formulation  $M_{n+1}X_nT_x$ , where M represents transition metal, X denotes carbon or nitrogen, and T depicts a surface functional group, such as hydroxyl, oxygen, or fluorine.<sup>4,5</sup> As a result of their exceptional electrical conductivity, extensive surface coverage, robust mechanical strength, and adaptable surface chemistry, MXenes are well suited for applications in energy storage,<sup>6</sup> catalytic processes,<sup>7</sup> environmental remediation,<sup>8</sup> and biomedical engineering.<sup>9</sup> Typically, MXenes are synthesized using conventional acid treatments to remove the A layer, allowing for control over surface terminations and functional groups.<sup>10</sup> Further enhancements in the characteristics of MXene nanosheets are achieved through techniques such as intercalation and exfoliation.<sup>10–12</sup> However, there is growing interest in developing green synthesis methods that utilize environment friendly chemicals. Alternative approaches like electrochemical etching, molten-salt etching, and alkali etching are being explored to improve the sustainability of MXene production.<sup>13,14</sup> Recent advance-

<sup>a</sup>Institute of Cardiovascular Sciences, St Boniface Hospital Albrechtsen Research Centre, Department of Physiology and Pathophysiology, Max Rady College of Medicine, Rady Faculty of Health Sciences, Biomedical Engineering Program, University of Manitoba, Winnipeg, Manitoba, R2H 2A6, Canada.

E-mail: [sdhingra@sbrcc.ca](mailto:sdhingra@sbrcc.ca)

<sup>b</sup>Institute of Atomic Physics and Spectroscopy, University of Latvia, Jelgavas iela 3, Riga, Latvia, LV-1004

<sup>c</sup>Biomedical Research Center, Sumy State University, Kharkivska street 116, Sumy, Ukraine, 40007

<sup>d</sup>Materials Research Center, 19/33A Yaroslav Val/O.Honchara str, Kyiv, 01034, Ukraine

†These authors contributed equally to this work.



ments include the use of organic Lewis acids in MXene synthesis, which allows for the direct production of MXenes with organic terminal groups, enhancing colloidal stability and electrocatalytic properties.<sup>15,16</sup> Additionally, low-cost synthesis methods, such as using titanium oxide instead of pure titanium, have been introduced to reduce costs and safety risks.<sup>17,18</sup> In our lab, we have reported the development of tantalum carbide ( $Ta_4C_3T_x$ ) MXenes with high efficiency and purity using a fluoride-free cost-effective protocol, enriched with bioactive functional groups, and stable surface  $TaO_2$  and  $Ta_2O_5$  functionalization.<sup>19</sup> The effectiveness of MXenes in different applications is heavily dependent on their structural, morphological, and chemical characteristics. Therefore, it is critical to examine and understand the properties of MXenes using methods including electron microscopy for morphology, X-ray diffraction to understand structural composition, and Raman spectroscopy to evaluate surface chemistry, which provide great insight for the compounds.<sup>20</sup> Precise control over synthesis parameters, including temperature and holding time, is crucial for achieving the desired structure and composition.<sup>21,22</sup> For instance, in synthesizing  $Ti_3C_2Cl_x$  MXene using molten salt, careful management of molar ratios and synthesis conditions is vital to obtaining a complete layered structure and controlled surface modifications.<sup>23,24</sup>

In the biomedical field, MXenes have demonstrated significant potential due to their biocompatibility, biodegradability, and hydrophilicity. Their large surface area and strong near-infrared (NIR) absorbance characteristics drive their employment in the wide area of biomedical applications, including photothermal therapy and bioimaging.<sup>25,26</sup> MXenes have also been explored for drug delivery, tissue engineering, biosensing, and theranostics, which integrates therapeutic and diagnostic functions.<sup>27</sup> Their ability to be functionalized with polymers enables controlled and targeted drug release, while in tissue engineering, MXenes are utilised to construct scaffolds that enhance cell growth and function. Their mechanical properties, such as strength and flexibility, make MXenes suitable for use in implants and wearable biomedical devices. Moreover, their conductive properties also make MXenes ideal for biosensing and bioimaging applications, as they can efficiently transduce signals, making them valuable for neural interfaces and diagnostic tools.<sup>3,28,29</sup> Additionally, the photothermal properties of MXenes are particularly beneficial for cancer therapy, where they can convert light into heat to destroy cancer cells.<sup>30</sup>

Despite their promising attributes, the biomedical application of MXenes is not without challenges. Stability in physiological conditions and potential cytotoxicity are critical concerns.<sup>31</sup> To address these issues, surface modification techniques are being developed to enhance the *in vivo* efficiency and reduce the toxicity of MXenes.<sup>32,33</sup> Integrating MXenes with polymers can improve their stability and functionality in biological environments, addressing the challenge of maintaining stability.<sup>34,35</sup> However, in order to fully exploit MXenes' biomedical potential, the challenges related to synthesis and functionalization must be overcome. Ensuring consistent

quality in large-scale production and controlling surface chemistry are vital for the successful integration of MXenes into clinical settings. Additionally, careful consideration of regulatory, ethical, and safety aspects is necessary to ensure that MXenes are safe and effective for long-term use in humans.

This review highlights the transformative potential of MXenes across various domains, including medical diagnostics, tissue engineering, and infectious disease management (Fig. 1). Wearable sensors can be enhanced with MXenes to offer improved sensitivity and speed, while their application as contrast agents for MRIs and CT scans for cancer therapy also offers enhanced sensitivity and speed. In tissue engineering, MXenes facilitate bone regeneration, soft tissue repair, and organ-on-a-chip platforms. Furthermore, MXenes contribute to antimicrobial surfaces, viral inactivation, and immune modulation, providing innovative solutions against infectious diseases. Additionally, the review also discusses the limitations of MXenes that are preventing their application in a clinical setting. In conclusion, as this field rapidly evolves, this overview highlights the significance of MXenes in advancing healthcare.

## 2. MXenes in next-generation medical diagnostics

MXenes exhibit outstanding electrical conductivity, large surface area, tunable chemical composition, and biocompatibility, proving useful for a wide variety of biomedical applications, including diagnostics.<sup>36</sup> One of the primary applications of MXenes in medical diagnostics is in the development of biosensors. MXene-based biosensors have shown remarkable potential due to their high sensitivity and specificity in detecting various biomarkers and pathogens. These sensors leverage the electrochemical properties of MXenes to translate molecular recognition events into detectable signals, enabling the ultrasensitive detection of major biological targets.<sup>37,38</sup> The incorporation of MXenes into biosensor designs enhances their performance, stability, and antifouling capabilities, making them ideal for point-of-care diagnostic applications.<sup>39,40</sup> Also, in cancer diagnostics, MXene-based hybrid electrochemical sensors have been developed to detect cancer biomarkers with high precision. As a result of MXenes' superior conductivity and stability, these sensors improve the detection limits and reliability of cancer diagnostics, providing an early detection and monitoring tool for cancer.<sup>41,42</sup> Additionally, MXenes' optical properties, which can be enhanced through the incorporation of metal oxides, further expand their utility in diagnostic imaging applications, such as contrast-enhanced imaging techniques.<sup>43</sup> This section gives an overview of the benefits of MXenes in medical diagnostics-based applications.

### 2.1. MXenes as wearable sensors

Wearable biosensors have gained immense attention for their potential in real-time, continuous health monitoring, enabling



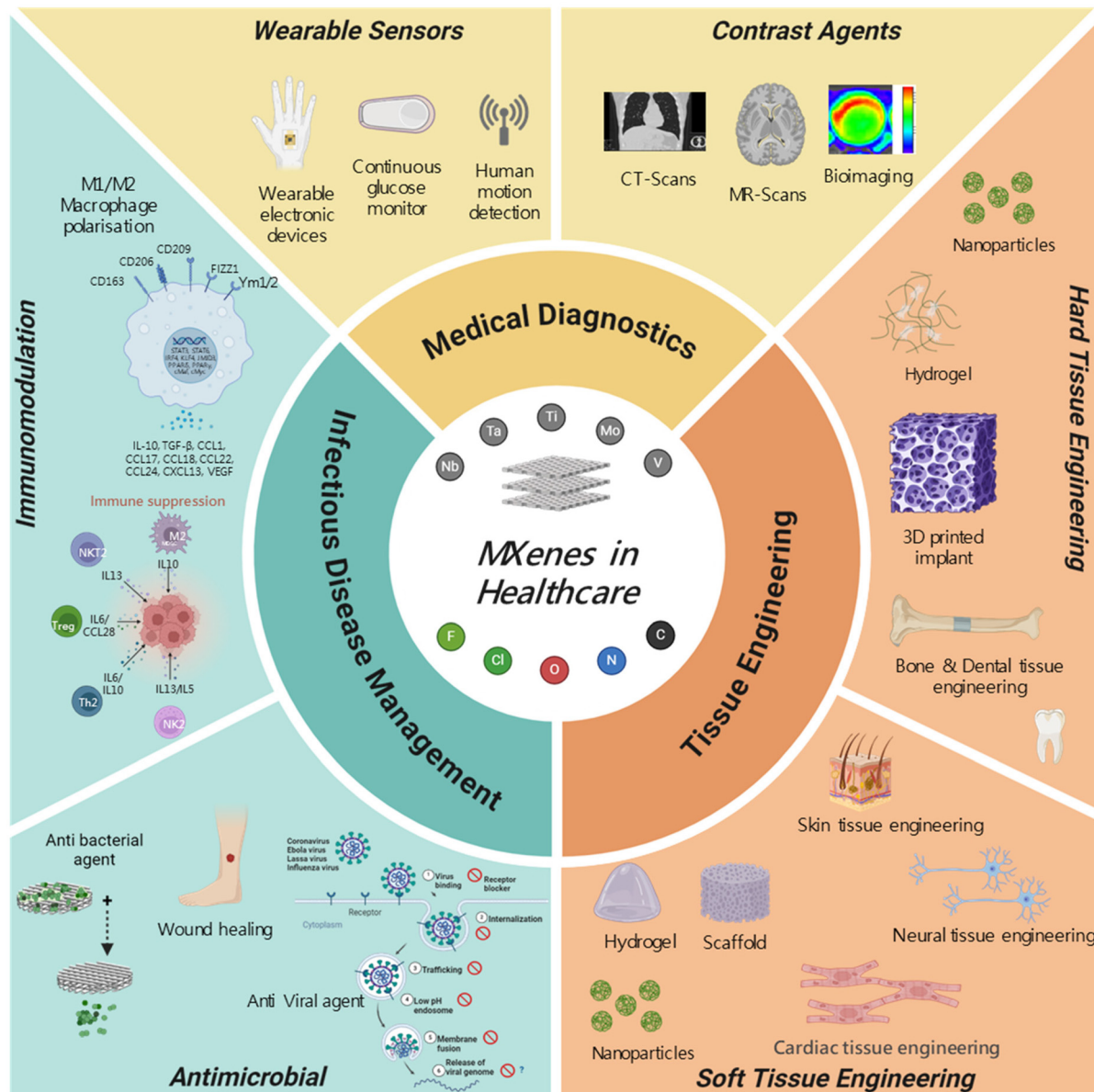


**Fig. 1** Schematic representation of the multifaceted applications of MXenes in biomedical fields. MXenes enhance the sensitivity and speed of wearable sensors, making them ideal for real-time health monitoring. In cancer therapy, MXenes function as effective contrast agents in MRI and CT scans, facilitating accurate diagnosis and treatment. MXenes play a vital role in tissue engineering by promoting both hard tissue regeneration and soft tissue repair. Additionally, MXenes contribute to innovative solutions for combating infectious diseases by enabling antimicrobial surfaces and supporting immune modulation, thereby showcasing their potential for a wide range of therapeutic applications. This figure was Created with [Biorender.com](https://www.biorender.com).

early diagnosis and personalized healthcare.<sup>44</sup> MXenes, with their remarkable electrical conductivity, mechanical flexibility, and large surface area, have emerged as exceptional materials for developing these advanced sensors. The high electrical conductivity of MXenes enables rapid signal transmission and enhances sensor sensitivity, allowing for accurate detection of physiological signals. Another key feature is their adjustable surface chemistry, which allows functionalization with groups such as  $-O$ ,  $-F$ , and  $-OH$ . This tunability enhances interaction with analytes, improving selectivity and enabling detection of

biomolecules, gases, and ions. For wearable applications, mechanical flexibility is also crucial, and MXenes excel in maintaining conductivity under repeated bending and stretching. Their layered structure allows seamless integration with flexible substrates, making them highly suitable for body-conformable sensors. Additionally, their hydrophilic nature facilitates stable dispersion in aqueous environments, improving adhesion to biocompatible substrates and enhancing sensor performance.<sup>45-47</sup> These properties make MXenes particularly well suited for wearable biosensors, which require high sensi-

tivity, flexibility, and durability to operate reliably in dynamic, real-world conditions such as body movements and physiological changes.<sup>48,49</sup> Consequently, in light of the intricate and multifaceted nature of their sensing mechanisms, these sensors have been extensively classified into two predominant categories, which are primarily identified as piezoresistive sensors and a combination of electrochemical and electrophysiological sensors. The application of the above wearable sensors will be discussed in detail within this section.

**2.1.1. Piezoresistive sensors.** One of the most significant and noteworthy applications of MXenes, a class of two-dimensional materials, within the realm of wearable biosensors is found in the development and utilization of flexible piezoresistive sensors (FPS), which are sophisticated devices that adeptly transform mechanical pressure exerted on them into corresponding electrical signals that can be measured and analyzed. The importance of these sensors cannot be overstated, as they play a critical role in the continuous and non-invasive monitoring of vital physiological parameters, including but not limited to heart rate, respiratory activity, and various forms of body motion that are essential for assessing an individual's health status. Furthermore, MXene-based FPS have demonstrated remarkable improvements in terms of responsivity, sensitivity, and signal accuracy, which collectively render them exceptionally well suited for integration into wearable health monitoring devices that aim to provide real-time data for personal health management and medical diagnostics.<sup>50</sup> A notable example is the production of  $Ti_3C_2T_x$  MXene and natural rubber (NR) composite fibers using a wet-spinning approach. MXene/NR fibers present tunable electrical conductivity along with stretchability, which can be tailored by adjusting the MXene loading. This adjustability makes them highly suitable for integration into textiles used in wearable sensors, as their electrical conductivity is responsive to strain variations, enabling accurate monitoring of body movements.<sup>51</sup> Moreover,  $Fe^{3+}$  ions significantly enhance the conductivity of  $Ti_3C_2T_x$  MXene nanosheet-based composite composed of nanoclay particles and *N*-isopropylacrylamide, reaching up to  $4.762\text{ S m}^{-1}$  upon surface interaction with MXene nanosheets.<sup>52</sup> The MXene-based sensor with a gauge factor of 1.28 displays a change in resistance 1.28 times for a given strain, a 120 ms response time enables the sensor to detect and respond to a change in strain within 120 ms, and a 400% working strain range allows the sensor to be stretched up to four times its original length without losing functionality.

MXene-based sensors, when integrated with deep learning algorithms, enable advanced posture recognition, real-time motion detection, and physiological monitoring, making them highly valuable in wearable technology. The MXene/polypyrrole (PPy) composite sensor exhibits high sensitivity ( $6.8925\text{ kPa}^{-1}$ ), rapid response (100 ms), and durability (5000 cycles, wash-resistant), making it ideal for human motion detection. It accurately monitors pulse and joint movements, integrates with deep learning for posture recognition, and holds great potential for wearable and intelligent sensing applications.<sup>53</sup> Beyond motion detection, MXene sensors demonstrate high

sensitivity in monitoring physiological signals, including speech as shown in an MXene/polydopamine composite film sensor and respiratory patterns as shown in TPU/MXene/Tungsten Disulfide Fibers, capable of accurately detecting vocalization and breathing, respectively, with high sensitivity.<sup>54,55</sup> Additionally, MXene-based sensor arrays have been employed for pressure distribution imaging and tactile sensing, providing high-resolution spatial pressure detection for electronic skin, robotic tactile interfaces, and human-machine interaction.<sup>56,57</sup> The ability of MXene sensors to accurately capture and analyze motion, pressure, and physiological signals underscores their potential for health monitoring, prosthetics, rehabilitation, and next-generation wearable technologies. These properties make MXene-based sensors versatile for monitoring human physiological signals in real time, including speech, respiration, and joint and muscle-related motion.

In the textile industry, MXene-treated fabrics have shown great potential due to their enhanced electrical conductivity, mechanical strength, thermal stability, water repellence, and antibacterial properties. These features pave the way for smart, multifunctional textiles that can be used for sustainable and medical diagnostics-based applications.<sup>58</sup> In a study, a  $Ti_3C_2T_x$ /(nonwoven fabric) composite exhibited high sensitivity ( $6.31\text{ kPa}^{-1}$ ), a broad sensing range (up to 150 kPa), fast response times (300 ms), and excellent durability, making it ideal for applications like wearable pressure sensors for healthcare monitoring<sup>59</sup> (Fig. 2). Moreover, in another study, by Zheng *et al.*, a conductive MXene-coated cotton fabric FPS-based sensor demonstrated a high sensitivity of  $5.30\text{ kPa}^{-1}$  in the low-pressure range (0–1.30 kPa), a wide detection range extending up to 160 kPa, and rapid response and recovery times of 50 ms and 20 ms, respectively, with excellent stability and durability over prolonged use. This versatile sensor can be employed for detecting and differentiating various physiological signals, such as finger movements, wrist pulses, and even early-stage Parkinson's static tremors.<sup>60</sup> Several MXene-based wearable piezoresistive sensors that are not covered in this section are summarized in Table 1. These wearable systems can benefit from the integration of artificial intelligence, enabling more advanced functionalities, such as predictive health monitoring and automated control of devices. Despite significant progress in the field, further research is needed to address challenges related to long-term durability, scalability, and integration in real-world wearable systems, ensuring MXene-based sensors reach their full potential in next-generation wearable technology.

**2.1.2. Electrochemical and electrophysiological sensors.** MXenes' broad surface area and extraordinary conductivity make them efficient for their application in electrochemical biosensors, which detect biomolecules such as glucose, lactate and other important biomarkers that are critical for continuous monitoring of health conditions like diabetes and metabolic disorders.<sup>70,71</sup> Recent progress in the field of MXene-based hybrid electrochemical sensors has resulted in extraordinarily substantial enhancements regarding the parameters of sensitivity, selectivity, and versatility, a phenomenon that has



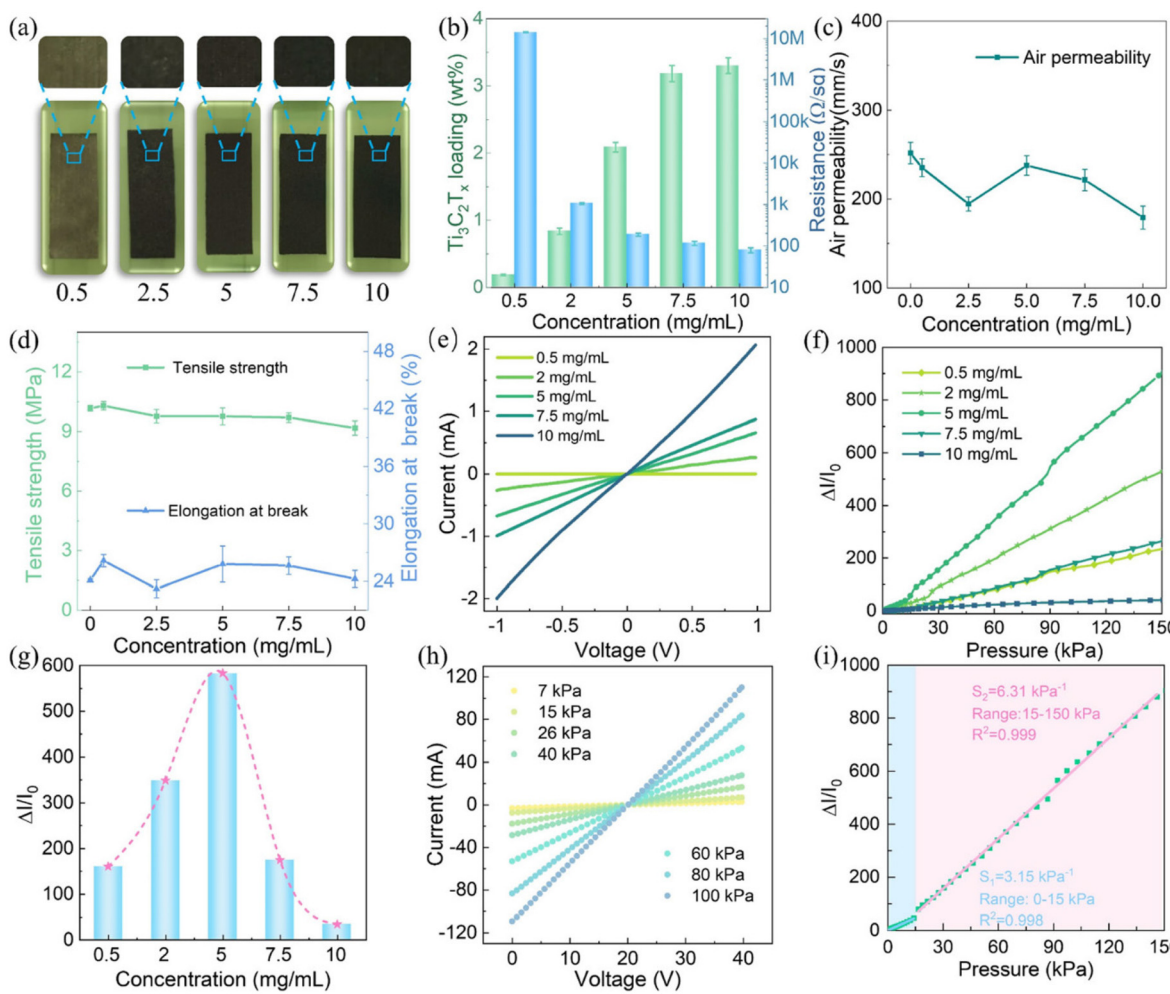


**Fig. 2** (a) Photographs of  $\text{Ti}_3\text{C}_2\text{T}_x$ @NWF samples impregnated using  $\text{Ti}_3\text{C}_2\text{T}_x$  dispersions with different concentrations. (b)  $\text{Ti}_3\text{C}_2\text{T}_x$  content and sheet resistance, (c) air permeability of  $\text{Ti}_3\text{C}_2\text{T}_x$ @NWF samples, and (d) mechanical properties of  $\text{Ti}_3\text{C}_2\text{T}_x$ @NWF samples as a function of the  $\text{Ti}_3\text{C}_2\text{T}_x$  dispersion concentration. (e)  $I$ – $V$  curves and (f) pressure–response curves for the  $\text{Ti}_3\text{C}_2\text{T}_x$ @NWF flexible pressure sensors. (g)  $\Delta I/I_0$  values and the corresponding fitting curve for  $\text{Ti}_3\text{C}_2\text{T}_x$ @NWF flexible pressure sensors at 100 kPa. (h)  $I$ – $V$  curves of the  $\text{Ti}_3\text{C}_2\text{T}_{x-5}$ @NWF flexible pressure sensors under various static pressures. (i) Sensitivity of the  $\text{Ti}_3\text{C}_2\text{T}_{x-5}$ @NWF flexible pressure sensor. (Reproduced with permission from ref. 59. Copyright © 2022, American Chemical Society).

arisen through the intricate amalgamation of MXenes with a diverse array of other nanomaterials, thereby engendering a pronounced synergistic effect that transcends the capabilities of the individual components. These innovative hybrid sensors have exhibited remarkable efficacy and performance across a wide spectrum of applications, which notably includes the real-time monitoring and detection of critical biological markers including glucose, uric acid, lactate, antioxidants and various cancer biomarkers that are essential for medical diagnostics and health monitoring.<sup>72</sup> For example, a high-sensitivity electrochemical sensor based on MXene/Cu-TCPP(Fe) was developed, as shown in the schematic Fig. 3A, allowing simultaneous detection of glucose and uric acid with unprecedented sensitivity and wide linear detection ranges, down to 1.88 aM for glucose, as shown in Fig. 3B.<sup>73</sup>

MXene-based sensors have demonstrated exceptional capabilities in noninvasive sweat analysis, enabling real-time moni-

toring of key metabolites for healthcare applications. These sensors offer high sensitivity, stability, and integration with wearable platforms, making them highly suitable for continuous health monitoring. For single-analyte detection, MXene-functionalized sensors have been developed to monitor critical biomarkers in sweat. A functionalized  $\text{Ti}_3\text{C}_2\text{T}_x$  MXene sensor achieved a 0.48  $\mu\text{M}$  detection limit for uric acid, surpassing some of the conventional uricase-based methods.<sup>74</sup> Similarly, MXene-functionalized PEDOT:PSS hydrogels were utilized to create a flexible glucose sensor with a 1.9  $\mu\text{M}$  detection limit, demonstrating excellent correlation with commercial glucose meters.<sup>75</sup> Additionally, a MXene/Prussian blue composite sensor exhibited high sensitivity for glucose ( $35.3 \mu\text{A mm}^{-1} \text{cm}^{-2}$ ) and for lactate ( $11.4 \mu\text{A mm}^{-1} \text{cm}^{-2}$ ) detection, key markers for physical performance and metabolic health.<sup>76</sup>

Beyond individual analytes, multi-analyte detection is crucial for comprehensive health assessment. A wearable

**Table 1** Overview of MXene-based piezoresistive wearable sensors, including key characteristics, and their respective applications in medical diagnostics

MXene-based composite	Key characteristics	Application	Ref.
2D $\text{Ti}_3\text{C}_2\text{T}_x$ nanosheets and 0D silicon nanoparticles (SiNPs)[MX@SiNPs]	<ul style="list-style-type: none"> <li>The MX@SiNPs cotton sensor exhibits exceptional sensing efficacy with a sensitivity of <math>12.23 \text{ kPa}^{-1}</math>, encompassing pressure (<math>8.8 \text{ Pa}</math>–<math>70 \text{ kPa}</math>), bending (<math>0^\circ</math>–<math>180^\circ</math>), and torsion (<math>0</math>–<math>628 \text{ rad m}^{-1}</math>).</li> <li>Maintains conductivity in wet and corrosive conditions for stable performance.</li> </ul>	Detects body motion in healthcare applications	61
( $\text{Ti}_3\text{C}_2\text{T}_x$ ) polyurethane (WPU)/polyacrylamide (PAM) dual-network hydrogels (PPM hydrogels)	<ul style="list-style-type: none"> <li>Durable under 1000 stretching cycles with 93.7% self-recovery and <math>639 \text{ kPa}</math> tensile strength.</li> <li>Reversible adhesion to multiple surfaces (skin, wood, PDMS) with <math>305.1 \text{ N m}^{-1}</math> adhesion strength.</li> <li>Ultrahigh sensitivity (GF up to 4720) with a wide strain range (<math>\sim 120\%</math>) and low detection limit (0.0645%).</li> <li>Durable, breathable, biocompatible, and antibacterial with rapid photothermal heating (<math>51^\circ\text{C}</math> in 60 s under NIR light).</li> <li>Wide working range (up to <math>39.28 \text{ kPa}</math>) with high sensitivity (<math>298.4 \text{ kPa}^{-1}</math>).</li> <li>Fast response (7 ms) and recovery time (16 ms).</li> </ul>	Monitors body and facial movements for healthcare applications	62
$\text{Ti}_3\text{C}_2\text{T}_x$ MXene nanosheets/WPU/chitosan (CS)/silver nanowires (AgNWs)	<ul style="list-style-type: none"> <li>Ultrahigh sensitivity (GF up to 4720) with a wide strain range (<math>\sim 120\%</math>) and low detection limit (0.0645%).</li> <li>Durable, breathable, biocompatible, and antibacterial with rapid photothermal heating (<math>51^\circ\text{C}</math> in 60 s under NIR light).</li> <li>Wide working range (up to <math>39.28 \text{ kPa}</math>) with high sensitivity (<math>298.4 \text{ kPa}^{-1}</math>).</li> <li>Fast response (7 ms) and recovery time (16 ms).</li> </ul>	Wearable human motion detection Photothermal therapy	63
$\text{Ti}_3\text{C}_2\text{T}_x$ MXene nanosheets/silk fibroin nanofiber (SF)	<ul style="list-style-type: none"> <li>Breathable, biocompatible, highly stable, and biodegradable.</li> <li>Ultrahigh sensitivity (up to <math>509.5 \text{ kPa}^{-1}</math>) with a low detection limit (1 Pa) and broad pressure range (up to 100 kPa).</li> <li>Stable over 10 000 cycles and recyclable.</li> </ul>	Detects tiny and large-scale movements Smart electronic skin for wireless biomonitoring	64
MXene-coated tissue paper (MTP)-with encapsulation layer made of polyimide (PI) film	<ul style="list-style-type: none"> <li>Broad sensing range (up to 80% strain) with high sensitivity (GF 2369.1) and ultralow detection limit (0.1538).</li> <li>Enhanced sensitivity and range with excellent cycling stability.</li> <li>High electrical conductivity with 81% elongation and 1.81 MPa mechanical strength.</li> <li>Self-healing restores 98.4% tensile strength and 97.6% conductivity without external stimuli, ensuring durability over multiple cut-heal cycles.</li> <li>Wide detection range (up to 70 kPa) with fast response (40 ms) and recovery (80 ms).</li> <li>Stable over 1000 fatigue cycles.</li> </ul>	Physiological signal monitoring	65
A-MXene-amino poly(dimethylsiloxane) (PDMS)	<ul style="list-style-type: none"> <li>High electrical conductivity with 81% elongation and 1.81 MPa mechanical strength.</li> <li>Self-healing restores 98.4% tensile strength and 97.6% conductivity without external stimuli, ensuring durability over multiple cut-heal cycles.</li> </ul>	Human motion detection with wireless biomonitoring system Wearable human motion monitoring	66
Reduced graphene oxide (rGO)/ $\text{Ti}_3\text{C}_2\text{T}_x$ MXene	<ul style="list-style-type: none"> <li>Wide detection range (up to 70 kPa) with fast response (40 ms) and recovery (80 ms).</li> <li>Stable over 1000 fatigue cycles.</li> </ul>	Artificial intelligence application Wearable strain sensor	67
Tannic acid (TA)/MXene/poly(hydroxyethyl acrylate) (PHEA)	<ul style="list-style-type: none"> <li>6 <math>\times</math> 6 sensing matrix for precise pressure mapping.</li> <li>High stretchability (<math>&gt;500\%</math>) with low hysteresis (<math>&lt;3\%</math>) and superior fatigue resistance (stable over 500 cycles at 300% strain).</li> <li>Strong adhesiveness, long-term stability (7 + days), and antifreezing capability (<math>-40^\circ\text{C}</math>).</li> <li>Precise strain sensitivity for small deformations and thermosensitivity for body temperature monitoring.</li> </ul>	Sensing matrix for pressure distribution Wearable electronic devices and electronic skin for human motion detection	68
		Human motion detection with body temperature sensing ECG signal detection	69

sensor integrating sodiated polymers and MXene nanosheets enabled sodium and creatinine monitoring, maintaining stability over 3000 cycles.<sup>77</sup> Moreover, a silane-functionalized MXene-PEGDA hydrogel facilitated the simultaneous detection of serotonin, uric acid and dopamine with detection limits between  $0.83 \mu\text{M}$ ,  $25.11 \mu\text{M}$  and  $2.55 \mu\text{M}$ , respectively, highlighting its potential for neurological and oxidative stress monitoring.<sup>78</sup> To enhance usability, MXene-based sensors have been integrated into wearable platforms such as epidermal patches and textile-based sensors. A nanoporous carbon-MXene composite epidermal patch was developed for real-time sweat glucose, pH, and temperature monitoring, while also capturing biopotential signals like ECG, demonstrating its

multipfunctionality.<sup>79</sup> Additionally, MXene-integrated carbon yarn sensors enabled dopamine detection in sweat with an impressive 316 pM detection limit and a broad linear range of  $1 \text{ nM}$ – $1 \mu\text{M}$ , and could be seamlessly sewn into clothing for continuous, noninvasive health tracking.<sup>49</sup>

In the detection of cancer biomarkers, MXene-based biosensors have proved particularly promising, enabling more accurate and sensitive cancer diagnostics. MXene- $\text{Co}_3\text{O}_4$  nanocomposites were used to develop a hydrogen peroxide sensor with a dynamic linear range of  $75 \mu\text{M}$ . The sensor can detect the hydrogen peroxide when it is present in very low concentrations up to  $0.5 \mu\text{M}$ , with accurate quantification from  $1.6 \mu\text{M}$  with consistent reliability. In cancer cell lines like



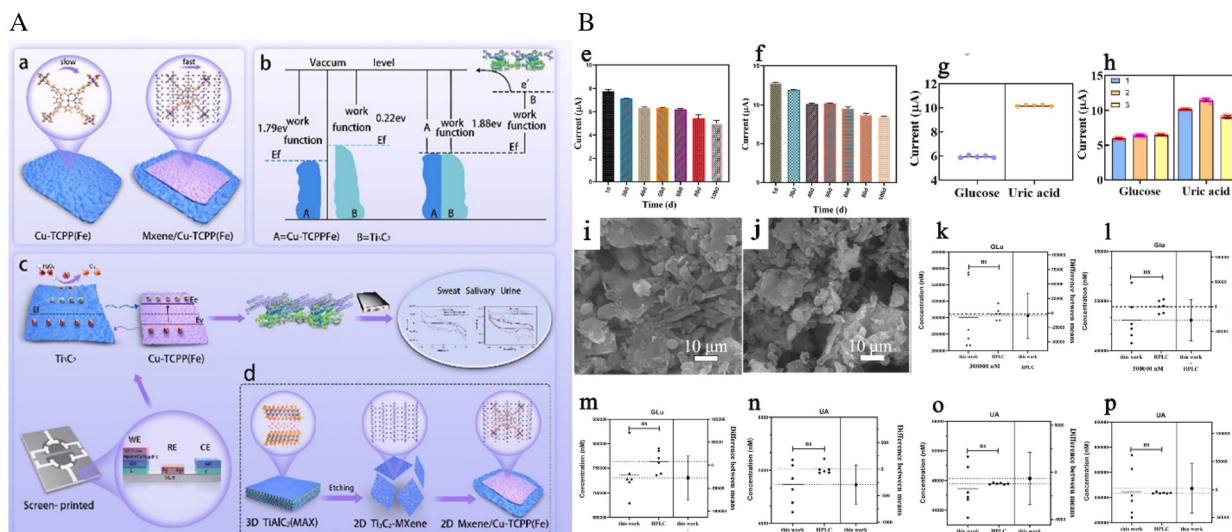


**Fig. 3** (A) Schematic illustration of the CuMxene interfacial interaction at heterointerface boosting electron transfer and electrocatalysis of (a) conductive networks for fast charge transfer and (b) dipole fields for directional charge transfer. (c and d) Schematic illustration of the MMs Paper-ECL Sensor synthesis. (B) Performance evaluation of MMs Paper-ECL. Stability of (e) Glu and (f) UA. (g) Repeatability and (h) reproducibility of Glu and UA. Weather resistance test of (i) before and (j) after. Methodological comparison of (k–m) Glu of 300 000, 500 000 and 700 000 nM, (n–p) UA of 5000, 50 000 and 500 000 nM. (Reproduced with permission from ref. 73. © 2024 Elsevier B.V. All rights are reserved, including those for text and data mining, AI training, and similar technologies).

MDA-MB-231 and DU145, this sensor successfully measured reactive oxygen species (ROS), as well as in healthy HaCat cells, showcasing its potential for real-time tracking of cancer progression and therapeutic responses.<sup>80</sup> Furthermore,  $Ti_3C_2T_x$  MXenes with various surface functionalization (O, F, and S) have been explored for the selective detection of volatile organic compounds (VOCs) associated with lung cancer biomarkers. Among these,  $Ti_3C_2O_2$  MXenes exhibited a particularly strong sensor response to VOCs like isoprene, benzene, cyclohexane, and formaldehyde. The strong physisorption between these VOCs and the MXene surfaces, driven by van der Waals interactions, influences the material's conductivity and sensor performance, making  $Ti_3C_2O_2$  a promising candidate for reusable VOC sensors aimed at early lung cancer detection through exhaled breath analysis. Studies further revealed that adsorption energies for selected VOCs on  $Ti_3C_2T_x$  MXenes ranged from  $-0.505$  to  $-3.49$  eV, indicating strong interactions conducive to high sensor sensitivity.<sup>81</sup>

The combination of MXenes' unique properties with functional materials continues to offer new opportunities for electrochemical biosensor development as seen in Table 2, improving the accuracy and efficiency in real-time healthcare monitoring. Despite these achievements, challenges remain, particularly in ensuring long-term stability, scalability for mass production, and maintaining high performance under varying environmental conditions. Future research is expected to focus on enhancing the functional properties of MXenes, optimizing fabrication processes, and integrating MXenes with artificial intelligence for smart healthcare and environmental monitoring systems. Nevertheless, the continued development of MXene-based biosensors holds great promise for revolutionizing sensor

technologies across healthcare, environmental, and wearable applications. In conclusion, MXenes hold immense promise for the development of wearable biosensors due to their superior electrical, mechanical, and chemical properties. From flexible piezoresistive sensors to multifunctional devices capable of detecting a range of human physiological signals, MXenes are at the forefront of next-generation wearable technology.

## 2.2. MXenes as contrast agents

MXenes have attracted significant scholarly interest as contrast agents in an array of biomedical imaging modalities, encompassing magnetic resonance imaging (MRI) and photoacoustic imaging.<sup>88,89</sup> Their distinctive characteristics, including elevated electrical conductivity, robust mechanical integrity, and adjustable surface chemistry, render them exceptionally advantageous for augmenting diagnostic precision and facilitating theranostic applications. This section discusses the role played by MXenes in different imaging modalities, their potential in multimodal imaging, and their integration into theranostic platforms.

MRI relies on the interaction of contrast agents with magnetic fields to enhance image contrast, and MXenes have been explored for both  $T_1$ - and  $T_2$ -weighted imaging. Their ability to be functionalized with magnetic nanoparticles enables them to act as efficient MRI contrast agents.<sup>30,88</sup> MXenes can serve as dual-mode MRI contrast agents, capable of both  $T_1$ - and  $T_2$ -weighted imaging. The ability to provide both imaging modes allows for more comprehensive diagnostic information. Moreover, MXenes can be engineered to respond to the tumor microenvironment, further improving MRI contrast. Dai *et al.*<sup>90</sup> reported that MnOx-functionalized  $Ti_3C_2$  MXenes could

**Table 2** Overview of MXene-based electrochemical/electrophysiological wearable sensors, including key characteristics, and their respective applications in medical diagnostics

MXene-based composite	Key characteristics	Application	Ref.
MoS <sub>2</sub> nanosheets/2D Ti <sub>3</sub> C <sub>2</sub> MXene	<ul style="list-style-type: none"> <li>High sensitivity (54.6 nA <math>\mu</math>M<sup>-1</sup>) with a low detection limit (4.2 <math>\mu</math>M) for ascorbic acid detection.</li> <li>2D/2D configuration provides multiple active sites for effective absorption and interaction.</li> </ul>	Sweat biosensing of ascorbic acid (AA) for its application in biomedical diagnostics	82
Ti <sub>3</sub> C <sub>2</sub> MXene/MoS <sub>2</sub> /carbon fiber paper	<ul style="list-style-type: none"> <li>Ultrahigh sensitivity for microRNA detection (as low as 3.16 aM) and high sensitivity for AA, uric acid (UA), and dopamine.</li> <li>Compatible with complex biofluids (serum, urine) with high reproducibility.</li> </ul>	Wearable health monitoring for biomedical diagnostics	83
TiO <sub>2</sub> /Ti <sub>3</sub> C <sub>2</sub> T <sub>x</sub> MXene/polyvinyl alcohol (PVA)/graphene oxide (GO)/screen-printed carbon electrode (SPCE)	<ul style="list-style-type: none"> <li>Wide detection range (0.01–60.0 <math>\mu</math>M) with strong <math>R^2</math> values (0.9968, 0.9936).</li> <li>Low detection limit (6 nM), high accuracy (97.6%–102% recovery), and low RSD (&lt;4.9%).</li> <li>Non-interferent detection in common urine components.</li> </ul>	Real-time health monitoring for clinical diagnostics	84
MXene (Ti <sub>3</sub> C <sub>2</sub> T <sub>x</sub> ) nanosheets/Pt nanoparticles	<ul style="list-style-type: none"> <li>Broad linear detection range (0–8 mmol L<sup>-1</sup>) for glucose under neutral pH.</li> <li>Non-enzymatic detection with Pt/MXene catalysis for enhanced stability.</li> <li>Conductive hydrogel ensures long-term durability by immobilizing the catalyst.</li> </ul>	Continuous glucose monitoring in diabetes management	85
Carbon-PEG/PEDOT : PSS or PPy/sodiated Ti <sub>3</sub> C <sub>2</sub> T <sub>x</sub> Mxene nanosheet.	<ul style="list-style-type: none"> <li>High stability over 3000 cycles with minimal electron transfer loss <i>via</i> sodium doping.</li> <li>Potentiometric sodium-ion sensing: 428 <math>\mu</math>F, 0.02 mV h<sup>-1</sup> signal drift.</li> <li>Voltammetric creatinine sensing: 402 <math>\mu</math>F, 0.008 <math>\mu</math>A h<sup>-1</sup> current drift, maintaining 0.01 <math>\mu</math>A h<sup>-1</sup> drift over 6 months for long-term reliability.</li> <li>Enhanced catalytic activity for glucose oxidation in PBS and artificial sweat.</li> <li>High sensitivity and low detection limit at a low operating potential (-0.24 V) to minimize interference.</li> <li>Stretchable electrode with mechanical stability (up to 30% strain) and strong <i>in vivo</i> correlation with blood glucose levels.</li> <li>Nonenzymatic detection for sensitive and stable UA monitoring.</li> </ul>	Dynamic sweat analysis in healthcare monitoring and environmental sensing	77
ZnO TPs (Tetrapods)/MXene (Ti <sub>3</sub> C <sub>2</sub> T <sub>x</sub> ) nanoflakes/GOx (glucose Oxidase)	<ul style="list-style-type: none"> <li>High sensitivity and low detection limit at a low operating potential (-0.24 V) to minimize interference.</li> <li>Stretchable electrode with mechanical stability (up to 30% strain) and strong <i>in vivo</i> correlation with blood glucose levels.</li> <li>Nonenzymatic detection for sensitive and stable UA monitoring.</li> </ul>	Real-time health monitoring in glucose biosensing	86
1,3,6,8-Pyrene tetrasulfonic acid sodium salt (PyTS)/Ti <sub>3</sub> C <sub>2</sub> T <sub>x</sub> MXene	<ul style="list-style-type: none"> <li>Wide detection range (5–100 <math>\mu</math>M) with a low detection limit (0.48 <math>\mu</math>M), outperforming uricase-based sensors.</li> <li>Impedimetric immunosensor for highly sensitive cortisol detection in sweat.</li> <li>Low detection limit (88 pM) with a linear range of 0.01–100 nM for real-time monitoring.</li> </ul>	<ul style="list-style-type: none"> <li>Non invasive UA monitoring</li> <li>Fitness monitoring</li> </ul>	74
Ti <sub>3</sub> C <sub>2</sub> T <sub>x</sub> MXene/laser-burned graphene (LBG) flakes/(PDMS)		Wearable electronic devices for cortisol monitoring	87

specifically enhance  $T_1$ -weighted MRI contrast in tumor regions, allowing for more precise imaging. In addition, superparamagnetic properties can be introduced by integrating iron oxide nanoparticles onto MXene surfaces. Fe<sub>3</sub>O<sub>4</sub>-functionalized Ti<sub>3</sub>C<sub>2</sub> MXenes exhibited high relaxivity values (394.2 mM<sup>-1</sup> s<sup>-1</sup>), making them effective  $T_2$ -weighted MRI contrast agents.<sup>91</sup> Similarly, in another study, Ti<sub>3</sub>C<sub>2</sub> MXenes have been integrated with gadolinium (Gd)-based polyoxometalates (POMs) producing multifunctional nanosheets that allow for both therapy and imaging, particularly in the context of breast cancer theranostics. These MXene-based materials have been shown to be effective in hyperthermal treatment, guided by MR/CT imaging, and in measuring real-time ROS in cancer cells, providing an innovative platform for tumor treatment and monitoring therapy efficacy.<sup>92</sup> The ability of MXenes to integrate multiple imaging modalities makes them powerful

tools for multimodal imaging and theranostics. Their combination of high X-ray attenuation, magnetic properties, and photothermal efficiency allows for the development of multifunctional imaging agents. In a study, a Ti<sub>3</sub>C<sub>2</sub>@Chitosan-MnFe<sub>2</sub>O<sub>4</sub> (TC@Ch-MFO) nanoplatform was developed, leveraging a Schottky junction to enhance ROS generation and chemodynamic therapy (CDT) under NIR excitation, as shown in Fig. 4. This multimodal platform integrates photothermal therapy and dual-mode MRI ( $T_1$  and  $T_2$ ) for both treatment and imaging, demonstrating excellent biocompatibility and negligible toxicity to healthy tissues. The platform offers a promising approach for synergistic cancer therapies, expanding the potential of MXenes beyond photothermal agents to multifunctional biomedical applications.<sup>93</sup>

Moreover, apart from cancer theranostics, MXene-based platforms have been investigated for their capacity to remove



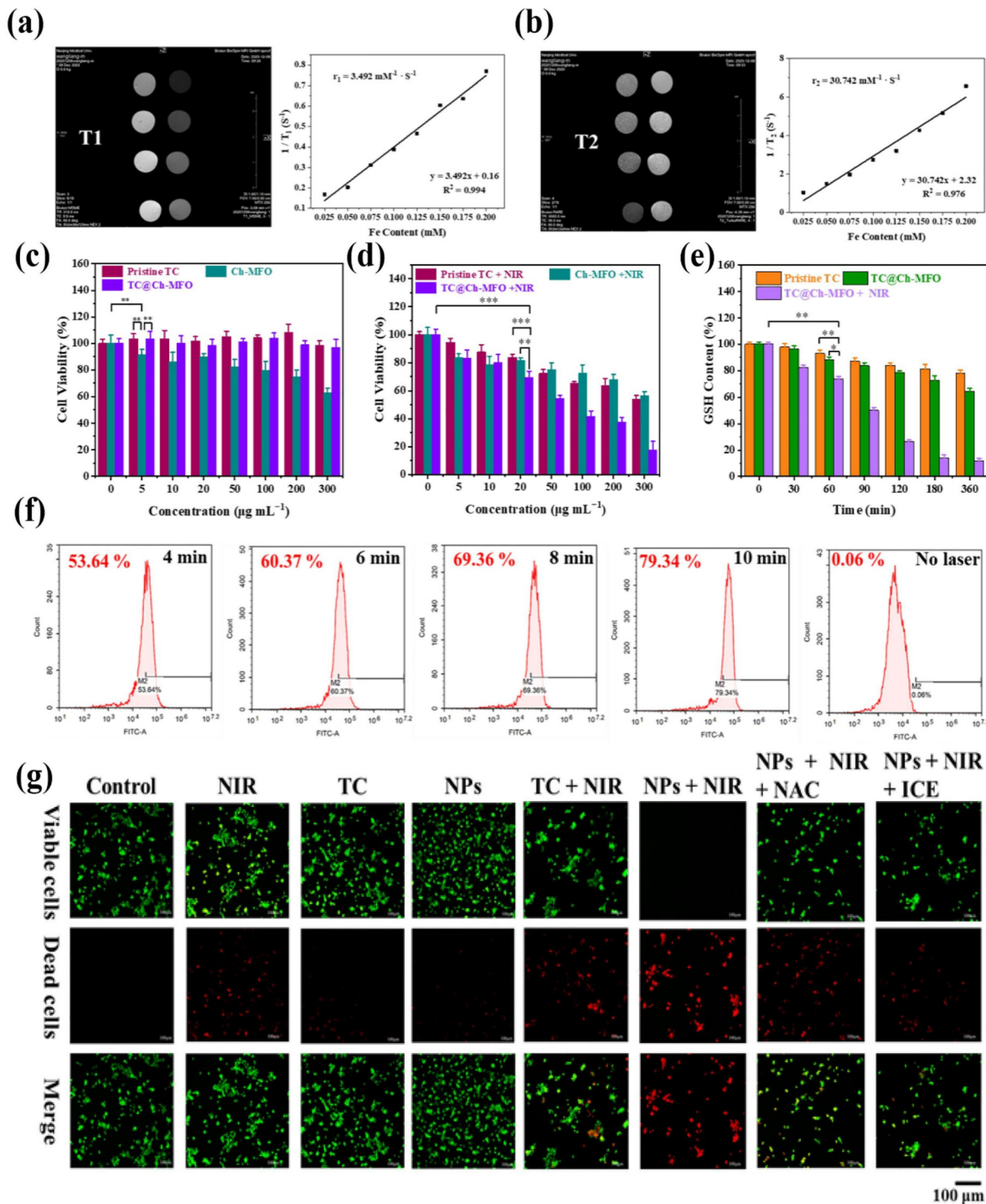


**Fig. 4** Bioimaging ability and Tumor Inhibition Efficacy of TC@Ch-MFO *in vitro*. (a)  $T_1$ -weighted MR phantom images of TC@Ch-MFO suspensions at different Fe concentrations. (b)  $T_2$ -weighted responding images of TC@Ch-MFO. (c) The cytotoxicity of material samples on HeLa cells at various concentrations without NIR irradiation. (d) Cell antitumor efficacy of samples under 10-minute irradiation of NIR irradiation at different concentrations. (e) GSH content in HeLa cells treated with different samples ( $100 \mu\text{g mL}^{-1}$ ). (f) Flow cytometry analysis of ROS production in TC@Ch-MFO incubated HeLa cells after NIR irradiation for various times. (g) Confocal fluorescence images of live (green) and dead (red) cells after different treatments. All the scale bars are  $200 \mu\text{m}$ ; ns, non-significant;  $**P < 0.01$ ;  $***P < 0.001$  (Reproduced with permission from ref. 93. © 2021 Elsevier B.V. All rights reserved).

uremic toxins from the blood, demonstrating strong adsorption for substances such as creatinine and indoxyl sulfate, with potential applications in kidney disease treatment.<sup>94</sup> This

study presents a novel covalent functionalization of  $\text{Ti}_3\text{C}_2\text{T}$  MXene flakes with diethylenetriaminepentaacetic acid and  $\text{Gd}^{3+}$  ions, imparting paramagnetic properties for  $T_1$ -MR



imaging. The approach enhances MXene stability, prevents oxidation, and improves cytocompatibility, while ensuring secure  $\text{Gd}^{3+}$  ion chelation. Additionally, the functionalized MXenes show high photothermal efficiency, expanding their potential for both bioimaging and photothermal therapy applications.<sup>95</sup>

MXenes have demonstrated significant potential as contrast agents for MRI, and photoacoustic imaging, offering enhanced imaging capabilities and the ability to integrate multiple modalities. Future research should focus on optimizing surface functionalization, improving biocompatibility, and developing scalable synthesis methods to enhance their applicability in biomedical imaging. With continued advancements, MXenes are poised to play a transformative role in next-generation medical imaging and nanomedicine.

### 3. MXenes in advanced tissue engineering

The unique properties, such as biocompatibility and tunable surface characteristics, of MXenes have made them excellent candidates for tissue engineering.<sup>96</sup> The two-dimensional structure of MXenes promotes cellular adhesion, growth and differentiation by facilitating enhanced intercellular communication between the MXene-based scaffold and biological system. Their surface terminations enable surface modification with bioactive compounds to promote specific tissue cellular specialization and to produce growth factors that drive tissue restoration. Their layered architecture facilitates efficient loading and effective encapsulation of bioactive agents, like growth factors and drugs, for controlled, sustained and targeted delivery. In addition to these biological properties that provide support and a favorable microenvironment for tissue regeneration, the thermal, electrical and optical properties of MXenes pave the way to creating smart biomaterials for tissue engineering applications.<sup>97</sup> This multifaceted nature of MXene-based scaffolds holds promise in advancing regenerative therapies, from organ transplantation and wound-healing to regeneration of diverse tissue types, encompassing both hard and soft tissues.

#### 3.1 MXenes in hard tissue engineering

Hard tissue engineering is a swiftly advancing field that aims to repair and regenerate damaged mineralized tissue like bone, cartilage and teeth. Scaffolds and biomaterials employed in hard tissue engineering are created to mimic the intricate architecture and composition of the mineralized tissues to promote cell adhesion, support tissue formation and integrate with the host tissue to instruct stem cells to improve tissue regeneration.<sup>98,99</sup> MXenes' intrinsic mechanical and electrical properties aid in mimicking the native physiological and electrical microenvironment of bone tissues, making them excellent candidates for bone tissue regeneration.<sup>100</sup> The osteogenic potential of multilayered  $\text{Ti}_3\text{C}_2\text{T}_x$  MXene films was investigated by culturing pre-osteoblastic cells on MXene films. MXenes significantly enhanced osteogenic differentiation by upregulat-

ing the mRNA levels of alkaline phosphatase (ALP), osteopontin (OPN) and osteocalcin (OCN) *in vitro*. When studied using a rat calvarial defect model, MXenes' ability to enhance osteogenesis and osteoinductivity *in vivo* when compared with clinically established titanium mesh was demonstrated.<sup>101</sup>

Three-dimensional (3D) MXene-based scaffolds have been employed to repair and reconstruct irregular-shaped bone defects. In this context,  $\text{Ti}_3\text{C}_2$  MXenes incorporated in hydroxyapatite and sodium alginate scaffolds were 3D printed and tested *in vitro* using bone marrow mesenchymal stem cells (BMSCs) and *in vivo* using critical-sized calvarial defects. The MXene composite exhibited high mechanical strength, uniform structure and excellent biocompatibility that promoted the bone regeneration both *in vitro* and *in vivo*, suggesting its promise in clinical bone defect treatment.<sup>102</sup> As seen in Fig. 5, the MXene scaffolds increased the mRNA expression of osteogenic genes. Similarly, 3D bioprinted BMSC-laden composite hydrogels comprising GelMA,  $\beta$ -TCP, sodium alginate and  $\text{Ti}_3\text{C}_2$  MXenes were personalized to target infected bone defects. The antibacterial, osteoinductive nature and photothermal ability of this composite enhanced bone regeneration and accelerated the resolution of infection, exhibiting its synergistic anti-bacterial and osteogenic effects.<sup>103</sup>

In addition to MXenes' excellent osteoconductive nature, MXenes exhibit excellent tumor ablation properties that can be tailored towards the use of MXenes in treating osteosarcoma. 3D printed  $\text{Ti}_3\text{C}_2$  MXene-loaded bioactive glass (BG) scaffold demonstrated the dual functionality of inducing photothermal hyperthermia to mediate bone-tumor ablation and bone regeneration.<sup>104</sup> Niobium carbide ( $\text{Nb}_2\text{C}$ ) MXene nanosheet-loaded BG scaffolds effectively promoted *in vitro* vasculogenesis of endothelial cells and stimulated angiogenesis and restrained the growth of osteosarcoma *in vivo*. This demonstrated the synergistic potential of MXene-loaded BG in addressing multiple aspects of bone health: inhibiting osteosarcoma, promoting osteogenesis and stimulating angiogenesis.<sup>105</sup> In addition to promoting osteogenesis, MXene-based hydrogels demonstrate promise in influencing macrophage polarization towards regulation of tissue regeneration processes. Incorporation of MXenes into the hydrogels imparts the essential electrical stimulation to remodel the osteoimmune microenvironment and reinstates the electrical milieu for effective bone regeneration.<sup>106</sup>

The osteoinductive nature of MXenes extends their application in guided bone regeneration for dental implant applications.  $\text{Ti}_3\text{C}_2\text{T}_x$  MXene-loaded epoxy resin composites were fabricated to prevent prosthodontic failure by harnessing MXenes' antibacterial activity and photothermal efficiency.<sup>107</sup> Integration of biocompatible MXenes into the resin increased the durability and mechanical properties of the composite, and effectively reduced bacterial colonization at the margins of the resin composite. This collectively contributed to the enhanced longevity and success of restorative dental treatments. In periodontal regeneration,  $\text{Ti}_3\text{C}_2\text{T}_x$  MXene incorporated into polylactic acid (PLA) with n-octyltriethoxysilane was developed. This composite matrix demonstrated excellent



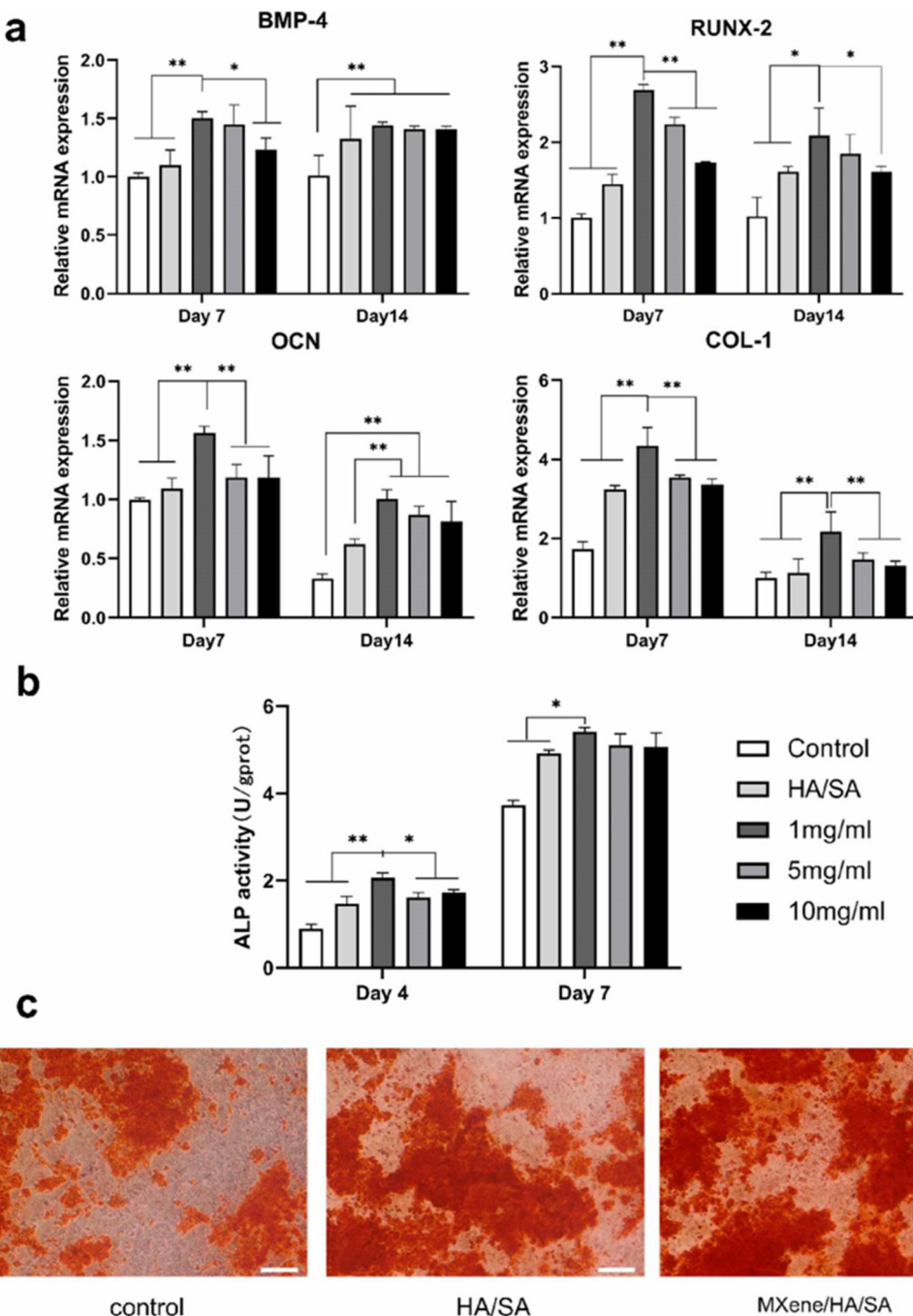


**Fig. 5** (a) Osteogenic gene expression of BMSCs in control, 3D-printed composite scaffold groups on days 7 and 14. \* $p < 0.05$ , \*\* $p < 0.01$ , \*\*\* $p < 0.001$ ,  $n = 3$ . (b) Quantitative ALP activity of BMSCs cultured on 3D-printed composite scaffolds for 4 and 7 d. \* $p < 0.05$ , \*\* $p < 0.01$ , \*\*\* $p < 0.001$ ,  $n = 3$ . (c) ARS staining of control, HA/SA, and MXene/HA/SA (1 mg ml $^{-1}$ ) at day 14 (scale bar: 100  $\mu$ m). (Reproduced with permission from ref. 102. © 2022 The Authors, Published by IOP Publishing Ltd).

mechanical characteristics compared with conventional PLA matrix and promoted the proliferation and differentiation of preosteoblasts.<sup>101,108</sup> By leveraging MXenes' ability to stimulate bone formation, 3D printed Ti<sub>2</sub>AlN MXene-loaded polycaprolactone (PCL) scaffolds were tested to repair tibial and maxillofacial bone defects (Fig. 6). The addition of MXenes into the composite scaffold resulted in enhanced mechanical pro-

perties, increased hydrophilicity and promoted osteogenesis via modulation of osteogenic signalling pathways, as revealed by transcriptomic analysis.<sup>109</sup>

The multifaceted properties of MXene-based composites make them promising materials for improving bone regeneration in bone tissue engineering and revolutionizing dental restoration procedures in regenerative dentistry.

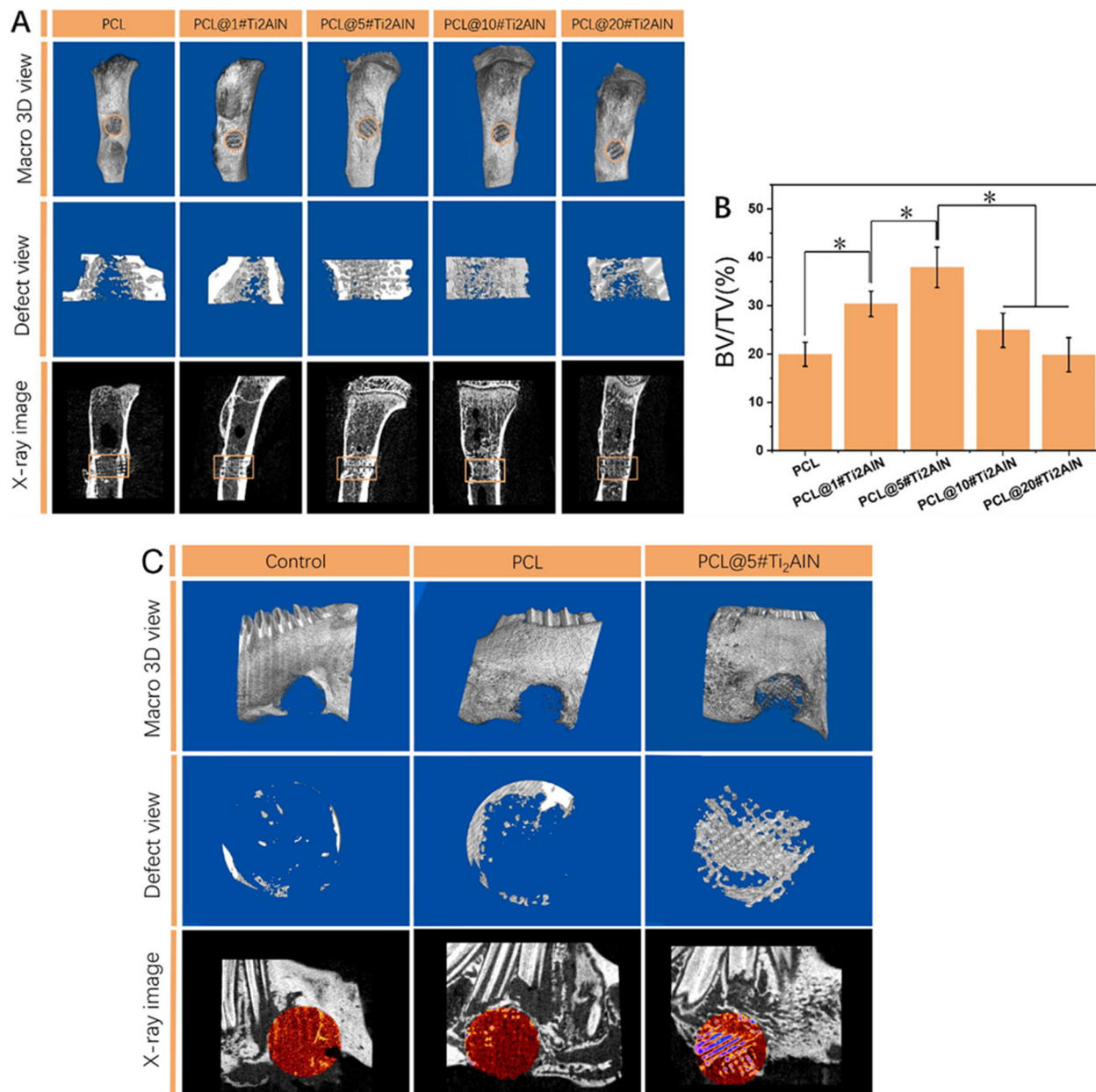


**Fig. 6** Repair of tibial and maxillofacial bone defects with different scaffolds. (A) Macro 3D view, defect view and X-ray image of tibial bone defects in rats, (B) BV/TV of tibial defect sites in rats,  $n = 3$ ,  $p < 0.05$ . (C) The repair of maxillofacial bone defects in rabbits by PCL and PCL@5#Ti<sub>2</sub>AIN scaffolds. (Reproduced with permission from ref. 109. © 2022 The Korean Society of Industrial and Engineering Chemistry. Published by Elsevier B.V. All rights reserved).

### 3.2 MXenes in soft tissue engineering

The human body consists of soft tissues including skeletal muscle, tendons, blood vessels, nerves, and organs including heart, brain, liver and kidneys. Upon chronic and acute injuries, these soft tissues and organs suffer severe damage, and their natural physiological healing and recovery mechanisms are often insufficient to restore normal function. This shortcoming has led to the development of clinical solutions using tissue engineering approaches, specifically soft tissue engi-

eering. Soft tissue engineering specializes in repair, regeneration and replacement of damaged soft tissues and organs by employing biomaterials that act as biomimetic extracellular matrix, support cell growth and facilitate tissue formation.<sup>110</sup> MXenes have gained significant attention in the field of soft tissue engineering due to their superior properties like excellent electrical conductivity, high surface area, mechanical flexibility and biocompatibility. The high surface area and electrical properties make MXenes valuable for enhancing cell adhesion and enabling transmission of electrical cues between

cells and conductive soft tissues, which are crucial for cell attachment, growth and regeneration.<sup>96,97,111</sup> Incorporation of conductive nanomaterials like MXenes into scaffolds and hydrogels enhances their electrophysiological properties, creating a 3D microenvironment that closely mimics the native tissue. This is particularly significant in the case of muscle, nerve and cardiac tissues, with limited regenerative capacity. Here, damage of these tissues results in the formation of non-functional scar tissue, where rebuilding the cell-to-cell electrical signalling is crucial for normal function restoration.<sup>112–114</sup> In addition to this, damaged tissue experiences a reduced supply of oxygen and nutrients due to disruptions in the network of blood vessels. MXenes have demonstrated potential in improving vascularization, which is crucial for the functional restoration of the extensive blood vessel network to ensure adequate supply of oxygen and nutrients to damaged cells and tissues.<sup>115,116</sup> Furthermore, the biocompatibility and anti-bacterial properties of MXenes show promise in contributing to a favourable healing microenvironment by reducing the potential risk of infections during tissue regeneration.<sup>28,117–119</sup> The tunable mechanical strength of MXenes also aids in synthesizing flexible composites with appropriate elasticity and compressive strength for various soft tissues.<sup>114,120,121</sup> Due to these properties, MXenes hold significant potential for regeneration and repair of various soft tissues including neural, connective, cardiac, vascular and skin tissue, and this is discussed in detail in the following sections.

**3.2.1 MXenes in neural tissue engineering.** Due to the inadequate regenerative capacity and complex neurophysiology of the nervous system post injury or neurological diseases, patients experience permanent functional impairments. To address this, neural tissue engineering (NTE) has emerged as a promising solution to create bioengineered scaffolds that support neural cell growth and restore damaged neural networks. Conductive biomaterials play a crucial role in nerve injury repair by providing essential electrical stimulation for promoting myelination and axonal regeneration.<sup>122</sup> MXenes' excellent electrochemical properties position them as ideal candidates for developing a conductive microenvironment to stimulate neural stem cell differentiation and facilitate functional integration of regenerated neural circuits.<sup>114</sup> MXenes' photothermal properties have garnered significant attention for the role they play in promoting optical modulation of neuronal electrical activity. This property enables precise modulation of the electrophysiology of dorsal root ganglion neurons, leading to the advent of non-invasive neuromodulation approaches in NTE.<sup>123</sup>

Studies show that  $Ti_3C_2T_x$  MXene nanosheets conjugated with other polymeric scaffolds and hydrogels have positively impacted neural stem cell proliferation and differentiation (Fig. 7).<sup>124</sup> These MXene composites establish a continuous network of conductive conduits to potentially replace the damaged peripheral nervous tissue and offer promise in spinal cord injury repair by overcoming the challenges posed by conventional biomaterials. They accelerate the regeneration of myelin sheaths and axons, and enhance calcium ion channel

activation and angiogenesis, collectively resulting in improved spinal cord regeneration.<sup>122,125</sup> Additionally, MXene-based hydrogels have been developed to serve as neural guidance conduits to re-establish the disrupted neural connection between regenerated neurons and injured axons. These hydrogels induced neural stem cell adhesion, promoted their proliferation, drove their differentiation and facilitated their maturation into functional neurons.<sup>126</sup>  $Ti_3C_2T_x$  MXene nanosheets were employed in developing 4D printed nerve guidance conduits to promote peripheral nerve regeneration *via* restoration of sciatic nerve function, improvement of nerve conduit conductivity and muscle morphology. This conduit–scaffold effectively drove enhanced nerve cell migration into the damaged nerve to repair the sciatic nerve injury.<sup>127</sup>

**3.2.2 MXenes in cardiac tissue engineering.** Cardiovascular disease is one of the leading causes of death worldwide, presenting a serious global health challenge. The limited regenerative potential of the adult heart and shortage of donors for heart transplantation have propelled medical professionals and researchers to explore alternative solutions. In response to this need, cardiac tissue engineering (CTE) has emerged as a promising field that focuses on developing functional cardiac constructs to repair or replace the damaged heart tissue. The use of conductive nanomaterials like graphene, carbon nanotubes and metal-based nanoparticles in CTE has efficiently enhanced the electrical conductivity of scaffolds, promoting cell–cell communication and conduction by mimicking the native myocardial tissue.<sup>128–130</sup> Following this trend, MXenes have also been employed in bioengineering cardiac constructs for cardiac tissue regeneration. Biocompatible polycaprolactone (PCL) scaffolds with MXenes were developed as conductive scaffolds to mimic the native myocardium.<sup>131</sup> It was observed that the conductivity of MXene-deposited electrospun PCL scaffolds ranged from  $5.22\text{ mS m}^{-1}$  to  $326.66\text{ mS m}^{-1}$ , showing resemblance to the  $1\text{ mS m}^{-1}$  conductivity found in normal myocardium. This finding suggests the potential use of these scaffolds to induce electrical signals across the damaged myocardium to improve the overall conductivity of the heart.<sup>132</sup> Another study involved the use of MXenes to enhance the electroconductive effects of biocompatible, conductive, adhesive hydrogel composed of gelatin and dextran aldehyde. In this study, the hydrogel upregulated the expression of connexin 43 and improved cardiomyocyte beat rate. *In vivo* results showed the potential of these hydrogels to be painted as a cardiac patch over the injured myocardium, stabilizing the beating epicardium by providing electrical conduction, mechanical support, improving tissue adhesion, reducing fibrosis and mitigating pathological remodeling of injured heart (Fig. 8).<sup>133</sup>

Another area in CTE that has garnered significant attention is the application of induced pluripotent stem cell-derived cardiomyocytes (iPSC-CMs). However, these iPSC-CMs are immature in nature in terms of morphology, structure, electrophysiology, calcium handling, contractility, mitochondrial and functional metabolism. This creates the need to develop strategies to get mature iPSC-CMs.<sup>134</sup> One such promising strategy



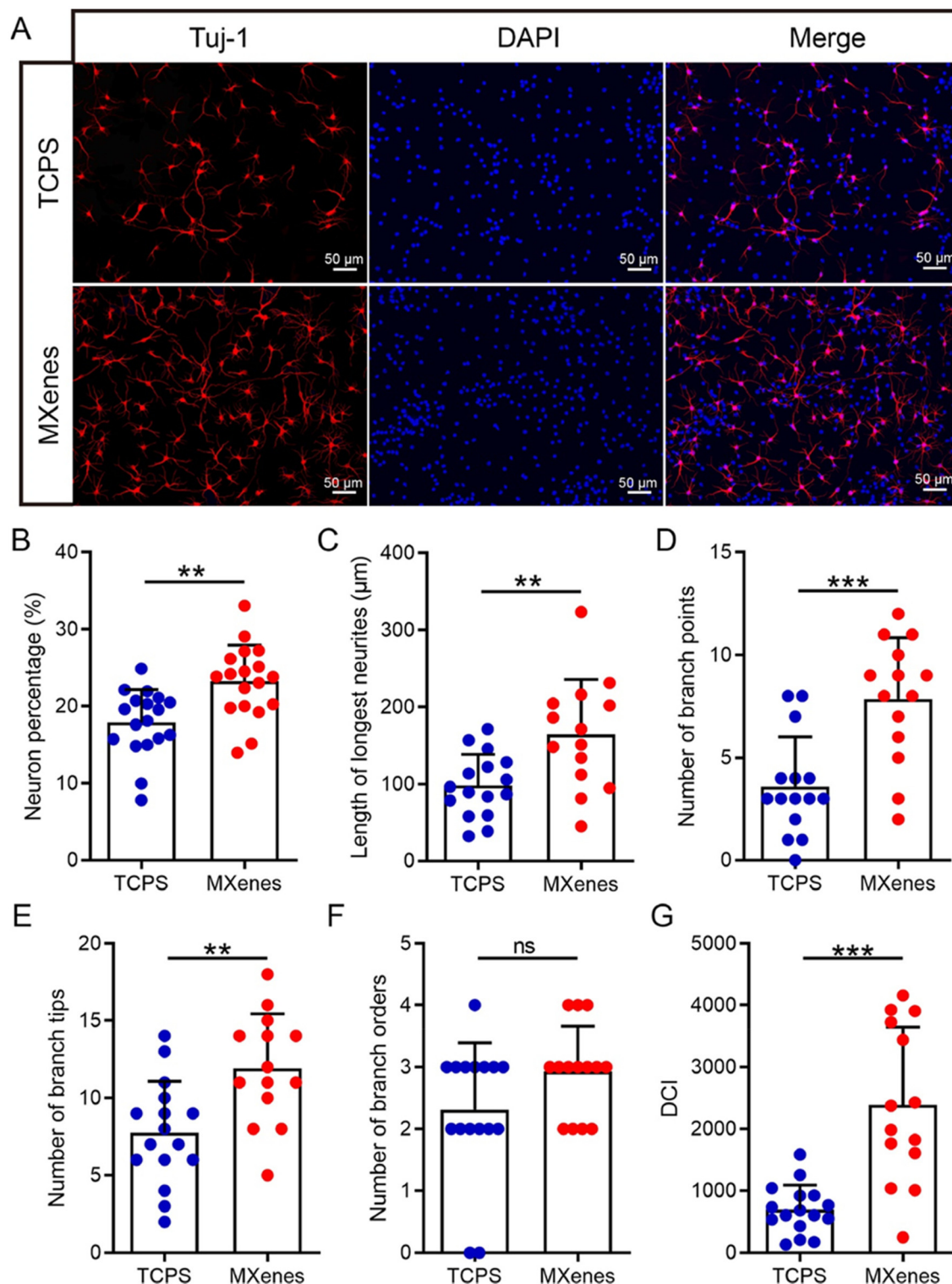


**Fig. 7** Effects of  $Ti_3C_2T_x$ MXene film on NSC differentiation. (A) Representative fluorescent images of NSC progeny cultured on  $Ti_3C_2T_x$ MXene film and TCPS substrate after NSCs were induced to differentiate for 7 days.  $\beta$ III-tubulin was stained red, and nuclei were stained blue. Scale bar: 50  $\mu$ m. (B–G) Histograms of the neuron percentage (B), the length of the longest neurites (C), the number of branch points (D), the number of branch tips (E), the number of branch order (F), and the dendritic complexity index (DCI) (G) from NSC-derived neurons. (Reproduced with permission from ref. 124. © 2020 Acta Materialia Inc. Published by Elsevier Ltd. All rights reserved).

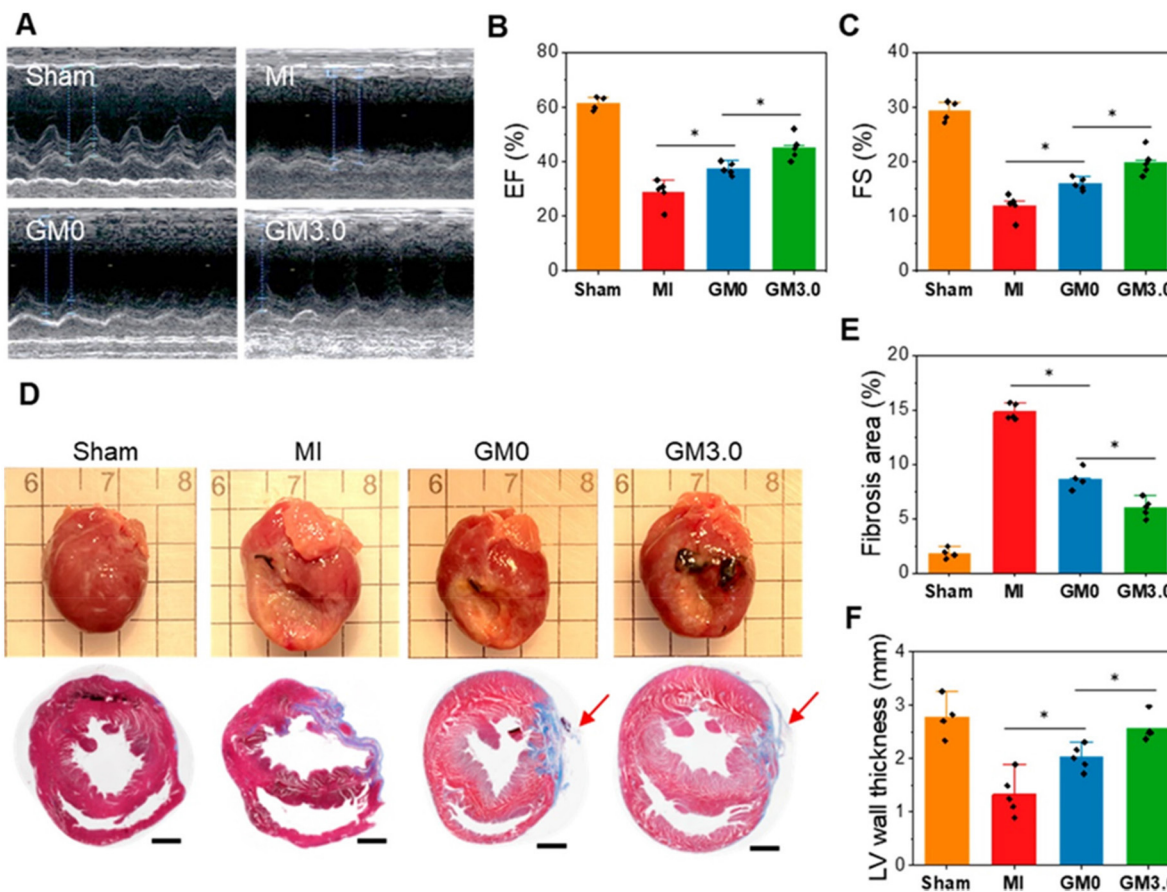


**Fig. 8** *In vivo* therapeutic effect of CAH cardiac patches on the left ventricle (LV) function and remodeling after myocardial infarction (MI). (A) Representative echocardiograms of the hearts 2 weeks after MI and treatment. (B) LV ejection fraction (EF) and (C) fractional shortening (FS) in various groups 2 weeks post-MI and treatment. (D) Representative gross anatomy of normal and injured rat hearts and Masson's trichrome staining images in various groups 2 weeks post-MI and treatment. Red arrows indicate the hydrogels remaining on the epicardium. Scale bar = 2 mm. (E) Fibrosis area (%) and (F) LV wall thickness (mm) of the rat hearts. Statistical significance was analyzed using one-way ANOVA followed by a Tukey analysis. \* $p < 0.05$ . (Reproduced with permission from ref. 133. Copyright © 2023, American Chemical Society).

involves the use of a conductive nanomaterial support matrix to provide an electrically biomimetic environment, to facilitate iPSC-CM maturation. MXene-loaded polyethylene glycol (PEG) hydrogels were developed in predesigned patterns with iPSC-CMs aligned on the hydrogels. These hydrogels positively impacted the iPSC-CMs' viability and maturity by enhancing synchronous beating and expression of cardiac markers: MYN7, SERCA2 and TNNT2.<sup>135</sup> Incorporation of MXenes into non-conductive hydrogels showed that MXenes enhanced the electrical signal transfer between CMs and improved calcium kinetics.<sup>121,136</sup> These findings show the potential of MXenes in improving the conductivity of scaffolds and hydrogels employed in CTE.

**3.2.3 MXenes in skin tissue engineering.** The goal of skin tissue engineering (STE) is to develop structural and functional alternatives for replacing, repairing and regenerating damaged or diseased skin. STE addresses the challenges involved in the complex process of wound healing and regeneration through bioengineered constructs. Wound healing is regulated by the endogenous direct current electric signals that inherently

occur at the wounded sites, due to differences in the transepithelial potential.<sup>137</sup> Research shows that conductive biomaterials can effectively mimic and enhance the natural electrical cues present in the wounded site. These biomaterials regulate cell behaviour towards healing by providing exogenous electrical stimulation and enhancing overall tissue repair outcomes.<sup>138,139</sup> MXenes are found to modulate wound healing by electrically stimulating skin cells. In this context, MXene-based biodegradable cellulose hydrogels were synthesized. The composite hydrogel possessed desirable electro-mechanical properties to influence the proliferation of cells towards accelerated wound healing, biodegradability and biocompatibility, both *in vitro* and *in vivo*. Specifically, the hydrogels enhanced collagen synthesis, angiogenesis, epithelial regeneration, and development of new vascularized connective tissue and blood vessels. This shows the synergistic potential of MXene-based composites in providing electrical stimulation for accelerated wound repair and healing.<sup>140</sup>

MXene-based hydrogels serve as effective drug delivery systems, harnessing their electrical property and stimuli-

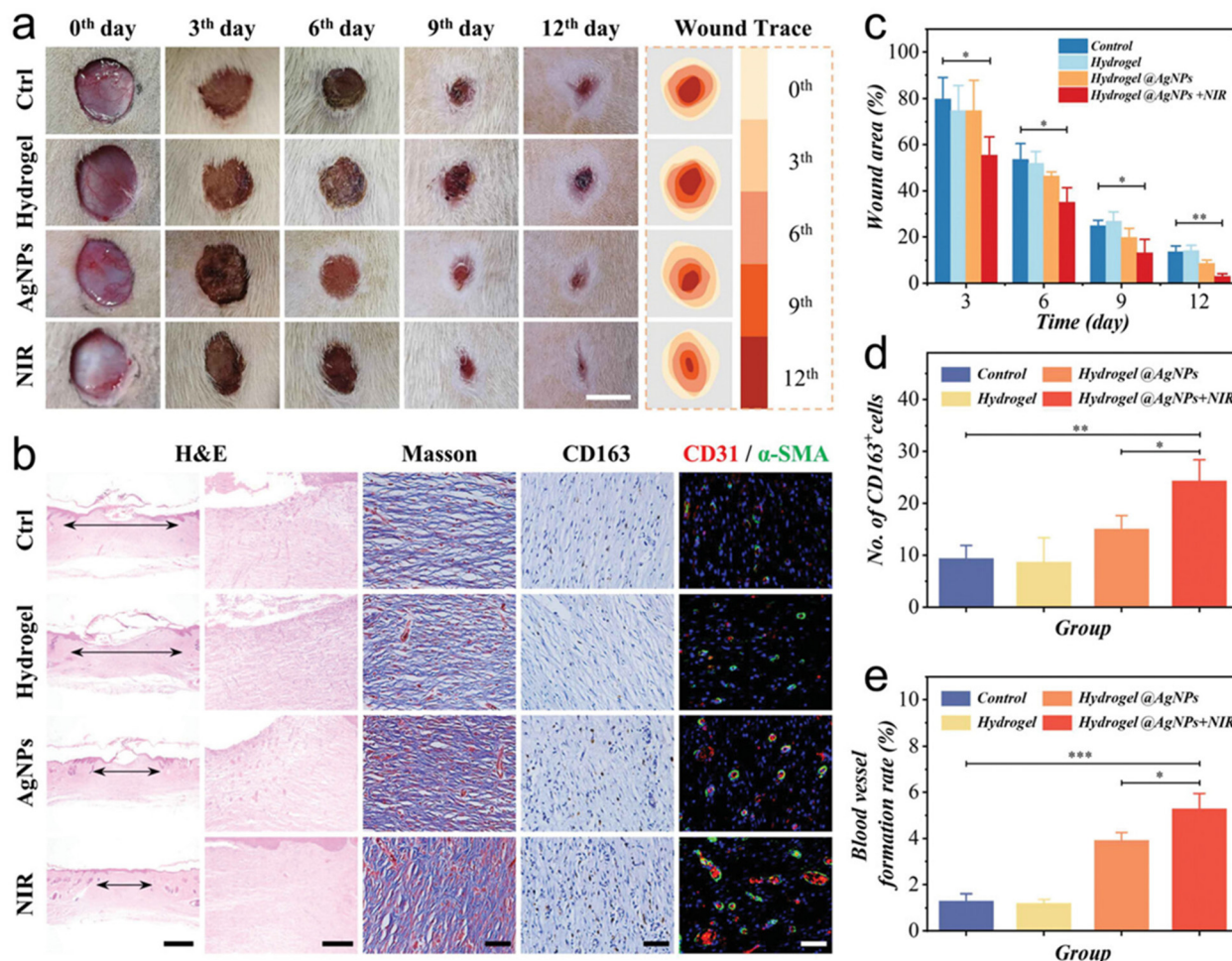


**Fig. 9** Therapeutic efficiency of the MXene-based hydrogel system in epidermal wounds. (a) Representative photos of the wounds treated with nonmaterial (Ctrl), MXene-based hydrogel (Hydrogel), Hydrogel@AgNPs (AgNPs), and Hydrogel@AgNPs + NIR (NIR) on days 0, 3, 6, 9, and 12. Scale bar is 1 cm. (b) Representative histological staining of wounds after 12 days. (c) Statistics of wound areas. Corresponding quantitative analysis of (d) the numbers of CD163 cells and (e) the blood vessel density. Data analyzed by one-way ANOVA ( $n = 3$ , \* $p < 0.05$ , \*\* $p < 0.01$ , \*\*\* $p < 0.001$ ). The scale bars are 1 mm, 200, 50, 50, and 100  $\mu$ m in (b), respectively. (Reproduced with permission from ref. 142. © 2021 Wiley–VCH GmbH).

responsive behaviour to aid in chronic wound healing.<sup>141</sup> This hydrogel system possesses multifaceted application in treating cutaneous and subcutaneous wounds in a rat model. By delivering drugs in response to photo/magnetic stimuli, these MXene-based systems show promise in clinical wound healing applications (Fig. 9).<sup>142</sup> Photothermally activated MXene-based systems show potential in wound healing, demonstrating robust antibacterial properties. These biomaterial systems effectively combat infections, reduce inflammation and can be used to develop infection-resistant wound dressings.<sup>143–145</sup> Vascular endothelial growth factor (VEGF)-loaded MXene-hydrogel exhibited exceptional photothermal effects and simultaneously promoted endothelial cell growth and blood vessel formation at the injured site. This system also influenced macrophage polarization towards the M2 phenotype and modulated the immune microenvironment at the wounded site.<sup>146,147</sup> MXene-based scaffolds exhibit anti-inflammatory capabilities by alleviating inflammation at the injured site and

thereby, promoting wound healing.<sup>148–150</sup> MXenes have shown significant potential in post-cataract surgery care by repressing heightened inflammation to promote wound healing. They reduced inflammatory responses, epithelial–mesenchymal transition and opacification in the affected lens to accelerate recovery in cataract patients.<sup>151</sup> Thus, by combining the electrical, photothermal, antibacterial and antimicrobial properties of MXene-based composites, they synergistically enhance wound healing processes like angiogenesis, collagen formation, fibroblast proliferation, endothelial cells, vascularization and inflammation mitigation in STE applications.

#### 4. MXenes in combating infectious and inflammatory diseases

Infectious and inflammatory diseases present two interlinked categories of global health challenges. Infectious diseases are

caused by pathogenic micro-organisms like bacteria, viruses, fungi and parasites that invade the host and pose significant damage to normal functioning. On the other hand, inflammatory diseases are caused by dysregulated immune responses, triggered by various factors like pathogens, cellular damage and toxic compounds. Inflammatory diseases encompass a wide range of conditions characterized by persistent and recurrent inflammation leading to chronic health problems.<sup>152</sup> Owing to the unique size, surface area, bioavailability and intrinsic antimicrobial properties of nanomaterials, nanomaterials have emerged as favourable tools to combat infectious and inflammatory diseases.<sup>153</sup> In the following sections, we discuss how MXenes play a pivotal role in developing treatments to combat infections, modulate inflammatory responses and promote tissue repair following infectious and inflammatory insults.

#### 4.1 MXenes in antimicrobial applications

Nanomaterials have revolutionized diagnostic and therapeutic approaches in treating infectious diseases by enhancing interaction with micro-organisms at the molecular level. Their size increases the bioavailability and biodistribution, while their surface properties, including charge and area, mediate superior interaction of nanoparticles with pathogens and enable efficient encapsulation of the drugs. This holds promise for enhanced bioactivity and targeted delivery of therapeutics.<sup>154,155</sup> The unique properties of MXenes offer the ability to traverse biological barriers for enhanced bioactivity for advancing diagnostics, treatment and targeted drug delivery biosystems.<sup>156</sup> MXenes' photothermal and photocatalytic property is harnessed in eliciting its anti-bacterial effects. Under UV irradiation, MXenes inactivate airborne bacteria with a photocatalytic performance of 30%.<sup>157</sup> MXene-based hydrogels exhibit exceptional synergistic antibacterial and photothermal performance under NIR exposure, and are employed in developing wound dressings.<sup>158</sup> Similarly, upon light exposure, MXenes elicit significant antibacterial activity up to 97% against *Escherichia coli* by the release of reactive oxygen species (ROS), initiating oxidative stress in the bacterial cells.<sup>159</sup> An in-depth study on the antibacterial effects of  $Ti_3C_2T_x$  MXenes was conducted, drawing comparisons with graphene oxide. This study elaborated the mechanism by which MXenes exert their antibacterial effects by damaging the bacterial cell wall to release cytoplasmic contents, to generate ROS and induce oxidative stress. Notably, this study revealed the size-dependent anti-bacterial efficacy of MXenes against different bacterial strains.<sup>160</sup>

In combination with other polymeric nanomaterials, modified MXenes have shown increased anti-bacterial effects. For instance, integration of delaminated MXenes with electrospun chitosan inhibited bacterial growth across various strains.<sup>161</sup> Likewise, MXene-based composite filter membranes play a prospective role in inhibiting waterborne bacterial growth and for application in anti-biofouling membranes in wastewater treatment systems.<sup>162</sup> Delaminated  $Nb_2CT_x$  and  $Nb_4C_3T_x$  inhibited bacterial growth at 94.2 and 96.1% respectively, based on their nanosheet size and atomic structure. As the MXene nanosheet size decreased, there was reduced bacterial cell viability and increased oxidative stress. This was attributed to the 2D mor-

phology of MXenes that facilitates the penetration of MXenes into the bacterial cell wall, making MXenes exhibit their anti-bacterial effect *via* physical damage and induction of oxidative stress.<sup>163</sup> These studies show that the antibacterial efficacy of MXenes is determined by their unique 2D morphology, nanosheet size and modifications, offering highly effective antimicrobial platforms for diverse applications.

As discussed earlier, building on the versatile applications of MXenes, MXenes are employed in sensor-based applications. In this regard, MXenes are used as biosensors for detection and screening of infectious pathogens.<sup>164</sup> Their alluring optical, fluorescent, surface plasmon resonance (SPR) and surface-enhanced Raman scattering (SERS) properties render them unique candidates for developing biosensors with high precision and efficiency. Electrochemically coated titanium MXene electrodes have demonstrated enhanced potential in sensing bacteria<sup>165</sup> and viruses like methicillin-resistant *Staphylococcus aureus* (MRSA),<sup>166</sup> zika virus,<sup>167</sup> SARV-CoV-2,<sup>168,169</sup> Middle East respiratory syndrome (MERS),<sup>170</sup> human papillomavirus (HPV)<sup>171</sup> and human immunodeficiency virus (HIV)<sup>172</sup> from diverse biological samples like human serum, saliva and cerebrospinal fluid. The exceptional biocompatibility and spectral stability of MXenes make them well suited for advanced biosensing applications. These characteristics enable MXenes to directly detect the interaction between aptamer and viral proteins, as well as bacterial components, thus improving the sensitivity of sensors.<sup>173</sup> Additionally, MXenes and MXene-based composites are employed as SPR<sup>174–176</sup> and SERS<sup>177,178</sup> biosensors to detect SARV-CoV-2 from human serum, saliva and other clinical specimens.

In the event of viral outbreaks, personal protective equipment (PPE) plays a vital role in protecting medical staff and containing the spread of infections. Recent advancements have led to progress in MXene-based graphene composites deposited on PPE *via* 3D printing. These MXene-based coatings serve as promising alternatives to traditional PPEs by enhancing the protective potential of PPE as reusable antimicrobial alternatives.<sup>179</sup> Microbial infections that are caused by bacteria or fungi cause critical complications in burns victims and severely injured patients. The widespread use of antibiotics has led to the advent of multi-drug-resistant bacteria, significantly diminishing the therapeutic efficacy of infected wound treatment. To address these increasing concerns, MXenes have emerged as promising antimicrobial agents and they are employed as nanozymes for CDT. The efficacy of these MXene-based antimicrobial mechanisms can be enhanced by the induction of NIR irradiation. Upon NIR irradiation, MXenes produce electrons and photothermal heating that synergistically amplify the CDT effect, showing the promise of MXene composites in combating antibiotic-resistant pathogens (Fig. 10).<sup>180</sup>

Thus, MXenes can be powerful antimicrobial agents by harnessing their inherent physiochemical properties of tunable chemistry, surface area, size, optical, electrochemical, plasmonic and photothermal effects. These diverse characteristics offer versatile platforms for the emergence of antimicrobial treatments, virus detection and the creation of advanced therapeutics to battle a wide variety of pathogens.



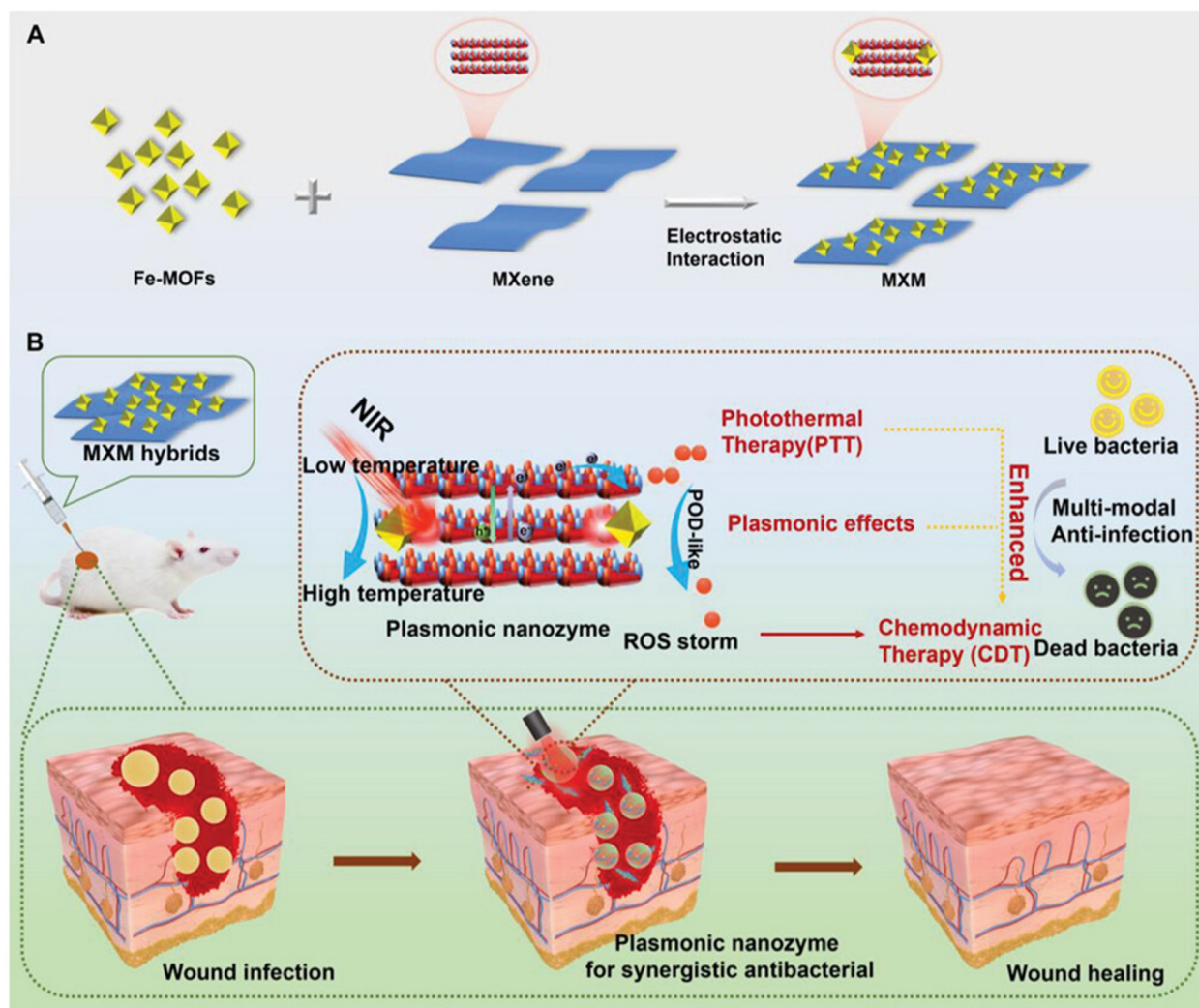


**Fig. 10** Schematic illustration of the synergistic antimicrobial therapy of MXM hybrids. (A) Synthesis of MXM hybrids; (B) the process and mechanism of PTT/CDT synergistic antimicrobial mechanism by NIR-induced plasmonic-enhanced MXM nanozymes. (Reproduced with permission from ref. 180. © 2023 Wiley–VCH GmbH).

## 4.2 MXenes in immunomodulatory applications

Research shows that nanomaterials have the ability to interact with the diverse immune population, functioning as immunomodulators, offering promising therapeutics for inflammatory conditions and inflammation-based diseases.<sup>181</sup> Carbon-based nanomaterials show anti-inflammatory properties, by reducing the expression of pro-inflammatory responses, production of pro-inflammatory cytokines and by delivering anti-inflammatory agents. The anti-inflammatory properties of nanomaterials have aided the modulation of signalling responses for improving tissue regeneration at the site of injury.<sup>182</sup> The conductive properties of MXenes, in combination with their distinctive physicochemical properties, regulate inflammatory responses to treat tumors, foster tissue regeneration and enhance graft acceptance upon implantation.

The surface-functionalized vanadium MXenes are employed as anti-inflammatory agents in colitis-associated colorectal

cancer. This type of cancer progresses by the development of chronic inflammation in the colon *via* the inflammation–dysplasia–carcinoma pathway. MXenes synergistically reduced ROS and pro-inflammatory cytokine levels with improved photothermal effects for tumor ablation in mice with colon cancer.<sup>183</sup> Niobium MXenes have been used to photothermally target osteosarcoma and promote angiogenesis at the infected site. Infiltration of immune cells into the MXene-based biomimetic scaffolds, after eliciting its therapeutic effects, leads to degradation of the scaffold, releasing calcium and phosphate ions to promote bone tissue biominerization promote osteogenesis. This type of immunotherapy for tumors establishes lasting immunological memory in the host to prevent tumor recurrence and provides long-term protection against cancer.<sup>105,184</sup>

MXene-based scaffolds and hydrogels exhibit tissue regenerative capability by regulating the immune microenvironment at the injury site. In the treatment of chronic diabetic wounds,

MXenes act as anti-inflammatory therapeutic agents to effectively scavenge excess ROS, mitigate persistent inflammation and promote wound healing.<sup>146,185</sup> MXene-based cardiac patches show promise in restoring the functionality of damaged myocardium by alleviating the inflammatory responses, promoting angiogenesis and supporting cardiac maturation.<sup>186</sup> MXenes are employed in bone regeneration therapies by manipulating the physiological conditions to promote M2 macrophage polarization. Combining the photothermal and immunomodulatory effect of MXenes, MXenes stimulate M2 macrophage polarization to enhance osteogenic differentiation of BMSC. This approach establishes the use of MXenes as osteoimmunomodulatory biomaterials in bone regeneration and orthopedic therapies.<sup>187</sup> Furthermore, MXene-based injectable neural interfaces were developed to overcome the limitation of conventional implantable neural interfaces. The redox stability of MXenes promotes nerve regeneration by mitigating inflammation at the implanted site to re-establish the electrophysiological neural signals.<sup>188</sup> This laudable versatility of MXenes to modulate inflammatory responses and promote tissue regeneration positions them as potential anti-inflammatory candidates in regenerative medicine.

MXenes are employed as promising orally administered antioxidant nanoagents to treat inflammatory bowel disease (IBD), a condition characterized by oxidative stress-induced chronic inflammation of the digestive tract.<sup>189</sup> MXenes are reported to be exceptionally effective in scavenging ROS, thereby promoting tissue regeneration by mitigating oxidative stress-induced damage. When orally administered, the negatively charged MXene nanosheets electrostatically bind to the positively charged inflamed colon tissue, initiating a cascade of anti-inflammatory effects: reduction of ROS, decrease in pro-inflammatory cytokine levels, promotion of M2 macrophage infiltration and increase in anti-inflammatory cytokine secretion. Through these mechanisms, MXenes effectively mitigate inflammation in the treatment of inflammatory gastrointestinal diseases. MXenes have been harnessed for their ROS scavenging abilities to synergistically elicit their photothermal/photodynamic effect to effectively inhibit bacterial growth.<sup>190</sup> MXenes extend their anti-inflammatory potential by suppressing the nuclear factor kappa-B (NF- $\kappa$ B) signalling pathway and ROS to effectively eradicate pathogenic bacteria and promote collagen deposition and angiogenesis (Fig. 11). This dual potential of anti-bacterial and anti-inflammatory properties makes MXene-based approaches a promising alternative in wound regeneration therapies.

Another inflammation-related disease condition where MXenes have shown significant potential is the mitigation of allograft vasculopathy. Allograft vasculopathy is a severe, accelerated form of atherosclerosis in transplanted organs and is the primary cause of acute graft rejection and subsequent transplant failure. MXenes, particularly titanium<sup>136,191</sup> and tantalum<sup>192</sup> carbide MXenes, have shown promise in preventing and treating allograft vasculopathy by modulating the immune response after transplantation. Studies have shown

that MXenes interact with endothelial cells to effectively inhibit the proliferation of T<sub>H</sub>1 lymphocytes, downregulate alloantigen presentation and reduce activation of pro-inflammatory cytokines. When tested using *in vivo* rat models, MXenes significantly reduced endothelial thickening and lymphocyte infiltration, and ameliorated smooth muscle cell integrity in transplanted aortic allografts (Fig. 12). These findings show that MXene-based immunomodulatory therapies can revolutionize regenerative and transplant medicine by preventing graft rejection and by improving the longevity of transplant outcomes. MXenes have been demonstrated to be valuable not only in biosensing detection of SAR-CoV-2 virus, but also inhibiting SAR-CoV-2 viral infections. Upon testing with 17 distinct immune subpopulations, MXenes reduced the release of pro-inflammatory cytokines and inhibited monocytes, highlighting their anti-inflammatory properties. Additionally, MXenes have the potential to disrupt different stages of the viral life cycle by affecting calcium signalling, INF- $\gamma$  responses and hindering virus internalization and replication. These findings underscore the importance of MXenes in antiviral-based immunomodulatory nanosystems.<sup>169,193</sup>

In conclusion, the versatile properties of MXenes—such as their tunable surface functionality, biocompatibility, and photothermal conversion efficiency—have made them applicable for biomedical applications ranging from drug delivery to tissue regeneration to advanced cancer theranostics and diagnostics.

## 5. Challenges in translating MXene-based interventions to clinical therapies

MXenes, a rapidly expanding class of two-dimensional nanomaterials, have shown profound potential in a variety of fields, especially in biomedicine. These materials have many unique properties that make them ideal for use in tissue engineering, biosensing, and theranostics as discussed above. In spite of their promise, MXenes face significant challenges for their transition from experimental research in the lab to clinical use in medicine. These challenges involve synthesis and scalability, biocompatibility, toxicity, and surface functionalization. At the same time, there are immense opportunities in regenerative medicine, personalized medicine, and theranostics that make MXenes one of the most promising material classes for future biomedical applications.

### 5.1. Synthesis and scalability

One of the foremost challenges in translating MXenes into clinical applications is the synthesis process. MXenes are typically synthesized by selectively etching the precursor materials, such as MAX phases, using hazardous chemicals like hydrofluoric acid (HF) or fluoride salts. This process poses significant environmental and safety concerns, especially for large-scale production. The toxicity of HF and the generation of



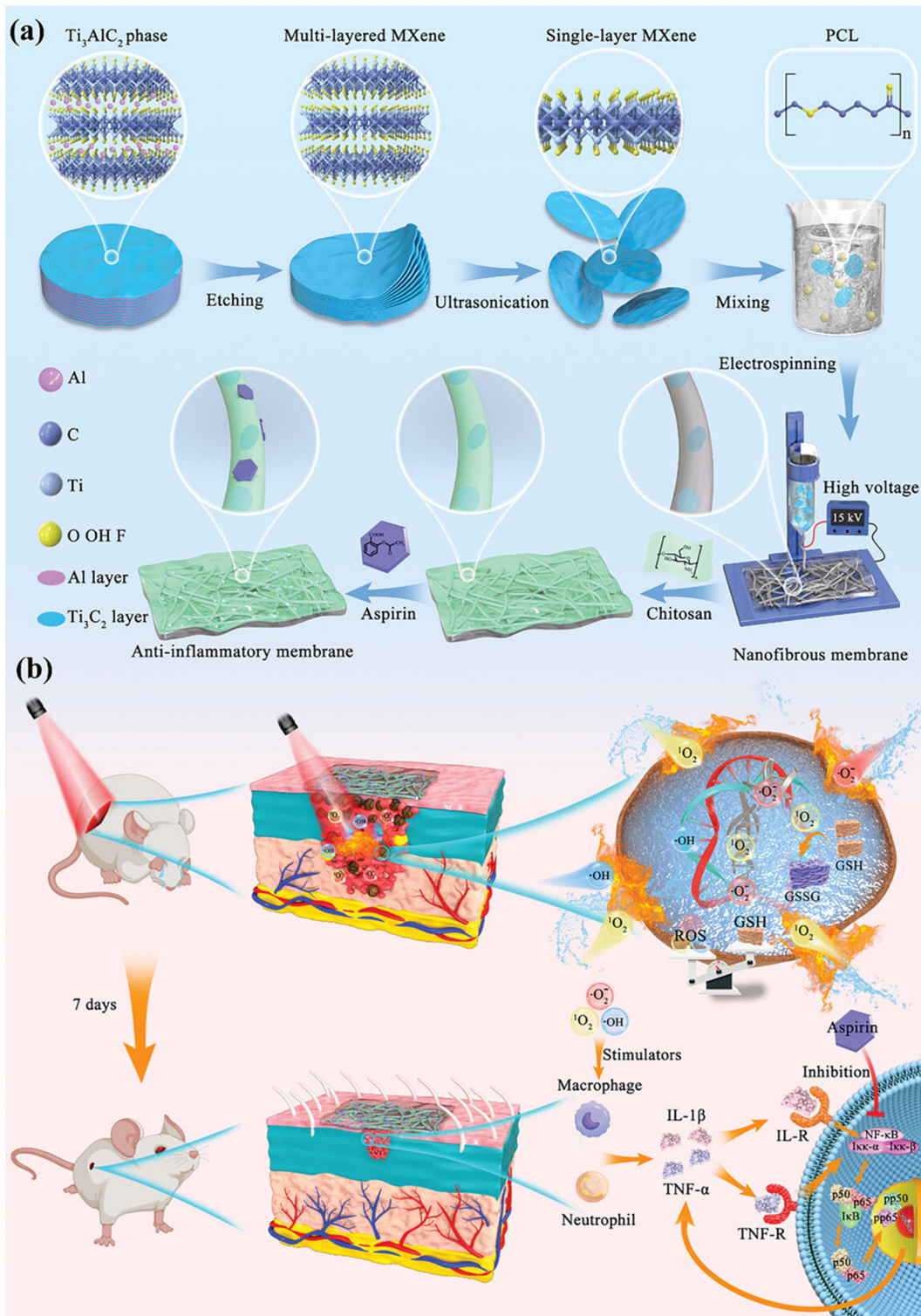


**Fig. 11** Schematic illustration of synergistic anti-bacterial and anti-inflammatory effects of MXene-decorated nanofibrous membrane; (a) preparation of the MXene-decorated nanofibrous membrane; (b) antimicrobial and infected wound repair effects by the resulting membrane via modulation of NF-κB Pathway. (Reproduced with permission from ref. 190. © 2023 Wiley–VCH GmbH).

chemical waste during synthesis hinder the commercial scalability of MXenes for biomedical purposes. As Oyehan *et al.* point out, developing safer, more sustainable, and scalable

synthesis methods is critical for advancing MXenes toward clinical applications.<sup>194</sup> In addition to environmental concerns, consistency in the properties of MXenes during syn-

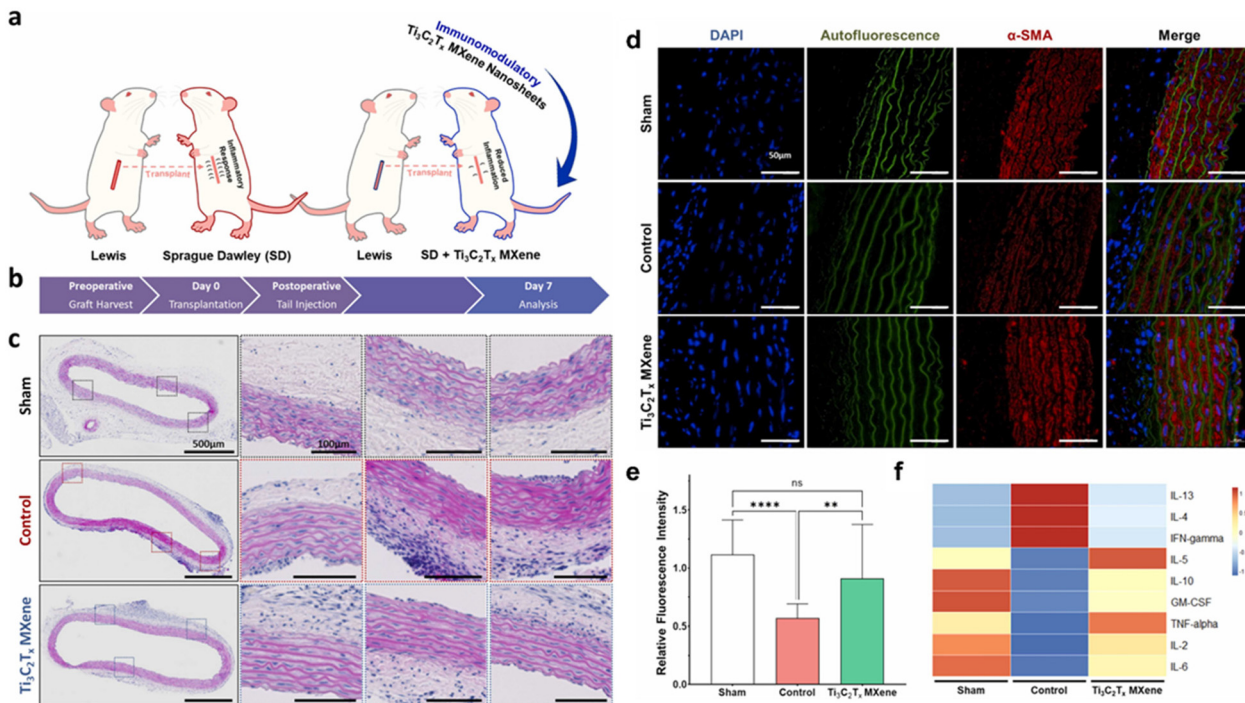


**Fig. 12** Treatment with  $\text{Ti}_3\text{C}_2\text{T}_x$  MXene nanosheets reduces allograft damage and inflammatory response in a rat model of cardiac allograft vasculopathy. (a and b) Briefly, segments of the thoracic aorta were harvested from male Lewis rats and transplanted as an interposition graft into the abdominal aorta of male Sprague Dawley (SD) rats. Animals received a  $1.5 \text{ mg kg}^{-1}$  tail vein injection of  $\text{Ti}_3\text{C}_2\text{T}_x$  MXene nanosheets immediately after transplantation. After 7 days, animals were euthanized, and tissues were collected for analysis. (c) On staining with hematoxylin and eosin, transplanted aortic segments from  $\text{Ti}_3\text{C}_2\text{T}_x$  MXene nanosheet-treated animals exhibited less endothelial thickening and adventitial inflammatory infiltration compared with control animals. Three to four animals were included per group. Immunohistochemistry and a multiplex ELISA were performed to quantify the degree of rejection against the allografts. (d and e) Immunohistochemistry was performed against alpha-smooth muscle actin ( $\alpha$ -SMA) as a marker for integrity of the vessel media. The abdominal aorta segments of each animal were normalized to a segment of the native thoracic aorta of the same animal. There was significantly decreased staining for  $\alpha$ -SMA amongst transplanted animals when compared with the sham animals. These changes were ameliorated in animals treated with  $\text{Ti}_3\text{C}_2\text{T}_x$  MXene nanosheets. (f) Multiplex ELISA against several cytokines was performed using blood plasma. As shown here, animals treated with  $\text{Ti}_3\text{C}_2\text{T}_x$  MXene nanosheets had a cytokine profile that resembled those of sham animals. In particular, there were lower levels of the pro-inflammatory cytokine interferon-gamma. Three to four biological replicates were included per group. (Reproduced with permission from ref. 191. © 2022 The Author(s). Published by Elsevier Ltd).

thesis poses another challenge. Achieving uniform quality in terms of size, shape, and surface chemistry is essential for biomedical applications, where reproducibility is key to ensuring safety and efficacy. Current synthesis techniques sometimes result in MXenes with varied thicknesses, surface defects, and functional groups, which can lead to inconsistent behavior in biological systems.<sup>195</sup> Therefore, improving the control over the synthesis process is vital for translating MXenes from bench to bedside.

## 5.2. Biocompatibility

The issue of biocompatibility is another significant hurdle for MXenes in clinical applications. While some studies have shown that MXenes exhibit low toxicity *in vitro* and in animal models, comprehensive *in vivo* studies are still required to assess their long-term effects in the human body. The interactions of MXenes with cells, tissues, and organs need to be understood in detail, as any potential cytotoxicity or immunogenicity could limit their use in clinical settings. Additionally, MXenes are prone to oxidative degradation, which could lead

to the release of toxic byproducts in biological environments. This necessitates extensive biocompatibility testing and potentially the development of surface coatings or functionalization to reduce toxicity.<sup>196</sup> Surface modifications have been explored to enhance the biocompatibility of MXenes. For instance, functionalization with biocompatible polymers or peptides can help to reduce their potential toxicity and improve their interaction with biological systems.<sup>197</sup> However, optimizing these surface modifications to achieve both biocompatibility and functionality remains a challenge. More research is needed to develop functionalization strategies that ensure that MXenes remain stable and safe for long-term use for humans without adverse effects.

## 5.3. Surface modification

A key factor in determining the behavior of MXenes in biological systems is their surface chemistry. MXenes are inherently hydrophilic, which can limit their dispersion stability in physiological environments, affecting their interaction with cells and tissues. To overcome this, effective surface functionalization is necessary



to improve their dispersibility and stability. Functionalizing MXenes with specific molecules, such as targeting ligands or polymers, can also enhance their ability to interact with particular biological targets, such as cancer cells or proteins, allowing for more precise therapeutic or diagnostic applications.<sup>198,199</sup> However, the functionalization of MXenes is still in its early stages, and many challenges remain in developing methods to control their surface chemistry and morphology consistently. Fine-tuning MXenes' surface properties to maintain their unique electronic and mechanical properties while also improving their biocompatibility and stability is a complex task. Furthermore, functionalization strategies must ensure that MXenes retain their therapeutic or diagnostic potential without compromising their performance in physiological environments. While MXenes do pose challenges, they present exciting opportunities for biomedical applications, particularly in tissue engineering, drug delivery, and theranostics.

## 6. Conclusion and future perspectives

MXenes have surfaced as highly advantageous materials for biomedical applications, especially in the realms of drug delivery, biosensing, tissue engineering, and oncological treatment. The distinctive physicochemical characteristics exhibited by MXenes, including elevated electrical conductivity, extensive surface area, and adjustable surface chemistry, render them exceedingly adaptable. Nevertheless, notwithstanding their promising capabilities, MXenes encounter numerous obstacles that necessitate resolution for their effective clinical application. These obstacles encompass inadequate physiological stability, apprehensions regarding cytotoxicity, challenges related to scalability, susceptibility to oxidative degradation, and implications for environmental sustainability. One of the primary limitations of MXenes in biomedical applications is their poor stability in physiological environments. Their high decomposition rate can reduce their effectiveness in drug delivery and limit their long-term performance in biological systems. A promising approach for enhancing stability is the formation of MXene-based composites with other two-dimensional materials, such as graphene or transition metal dichalcogenides. These hybrid materials have demonstrated improved drug release profiles and prolonged delivery in preclinical studies. Additionally, surface functionalization with functional groups such as hydroxyl ( $-\text{OH}$ ) and oxygen-containing moieties can improve MXene stability and facilitate better drug loading and controlled release.

Another critical challenge is the scalability of MXene synthesis. Current methods, such as chemical exfoliation, involve complex and expensive procedures that limit large-scale production. The development of cost-effective synthesis approaches, such as fluoride-free hydrothermal synthesis, can enhance the commercial viability of MXenes. Furthermore, advancements in automated and high-yield production techniques will be necessary to make MXenes more accessible for biomedical applications. Addressing scalability issues will be a

key factor in accelerating their transition from laboratory research to clinical applications.

While MXenes are generally considered biocompatible, their cytotoxicity and long-term biosafety remain concerns. Some studies have reported potential toxicity at higher concentrations or in specific biological environments. To ensure their safe use in clinical applications, rigorous *in vitro* and *in vivo* toxicity studies are essential. Standardized testing protocols must be developed to facilitate consistent evaluation across different studies and research groups. Additionally, surface modifications using biocompatible coatings with MXenes, such as polyethylene glycol or silicon dioxide, can help mitigate toxicity concerns, enhance biosafety and reduce their oxidation.

Pharmacokinetics also poses a significant challenge for MXene-based drug delivery systems. Poor targeting efficiency and limited circulation time in the body can reduce their therapeutic effectiveness. To address this, future research should focus on developing targeted drug delivery systems by functionalizing MXenes with targeting ligands, such as antibodies, peptides, or aptamers. Additionally, optimizing MXene size, surface charge, and hydrophilicity can improve their bio-distribution and circulation time, making them more effective in drug delivery and cancer therapy.

The environmental impact of MXene synthesis and disposal is another area of concern. Traditional synthesis methods rely on strong acids and high temperatures, which generate harmful byproducts. Additionally, the potential release of MXene nanoparticles into the environment poses risks that have not yet been fully explored. Future research should focus on developing green synthesis methods that minimize toxic waste and reduce environmental hazards. Additionally, studies on MXene biodegradability and long-term environmental fate are necessary to ensure their safe use and disposal.

Regulatory challenges also present a major hurdle for the clinical translation of MXene-based technologies. Currently, standardized safety and efficacy guidelines for MXenes in biomedical applications are lacking. Establishing regulatory frameworks and toxicity testing protocols will be crucial for obtaining clinical approval. Collaboration between researchers, clinicians, and regulatory agencies will play a pivotal role in addressing these challenges and accelerating the integration of MXenes into clinical practice.

In order to overcome these challenges and fully realize the potential of MXenes in advanced medical technologies, scientists, engineers and clinicians must work together as an interdisciplinary team. With continued research and development, MXenes could enact a transformative role in medicine, specifically in tissue engineering, sensor development, and theranostics, contributing to the future of personalized and regenerative medicine.

## Author contributions

This study was conceptualized and designed by KNA, LRS and SD; KNA, LRS, KD, VZ, OG, MP and SD conducted the litera-



ture search and prepared the initial draft; KNA, LRS and SD revised the manuscript. All authors read and approved the final manuscript.

## Data availability

No primary research results, software or code have been included and no new data were generated or analysed as part of this review.

## Conflicts of interest

The authors declare no conflict of interest to this work.

## Acknowledgements

This work was supported by funding from the Natural Sciences and Engineering Research Council (NSERC) of Canada to Dr Sanjiv Dhingra.

## References

- 1 M. Naguib, M. W. Barsoum and Y. Gogotsi, *Adv. Mater.*, 2021, **33**, 2103393.
- 2 R. K. Mishra, J. Sarkar, K. Verma, I. Chianella, S. Goel and H. Y. Nezhad, *Open Ceram.*, 2024, **18**, 100596.
- 3 I.-C. Lee, Y.-C. E. Li, J. L. Thomas, M.-H. Lee and H.-Y. Lin, *Mater. Horiz.*, 2024, **11**, 876–902.
- 4 A. VahidMohammadi, J. Rosen and Y. Gogotsi, *Science*, 2021, **372**, eabf1581.
- 5 M. Naguib, V. N. Mochalin, M. W. Barsoum and Y. Gogotsi, *Adv. Mater.*, 2014, **26**, 992–1005.
- 6 N. H. Solangi, R. R. Karri, N. M. Mubarak, S. A. Mazari and A. K. Azad, *J. Energy Storage*, 2023, **70**, 108004.
- 7 C. Xia, H. Ye, A. Kim, S. A. Namini, S. Li, S. A. Delbari, J. Y. Park, D. Kim, Q. V. Le, R. S. Varma, R. Luque, A. T-Raissi, H. W. Jang and M. Shokouhimehr, *Chemosphere*, 2023, **325**, 138323.
- 8 A. S. Jatoi, N. M. Mubarak, Z. Hashmi, N. H. Solangi, R. R. Karri, Y. H. Tan, S. A. Mazari, J. R. Koduru and A. Alfantazi, *Chemosphere*, 2023, **313**, 137497.
- 9 H. Li, R. Fan, B. Zou, J. Yan, Q. Shi and G. Guo, *J. Nanobiotechnol.*, 2023, **21**, 73.
- 10 B. Anasori, Y. Xie, M. Beidaghi, J. Lu, B. C. Hosler, L. Hultman, P. R. C. Kent, Y. Gogotsi and M. W. Barsoum, *ACS Nano*, 2015, **9**, 9507–9516.
- 11 T. Zhang, L. Pan, H. Tang, F. Du, Y. Guo, T. Qiu and J. Yang, *J. Alloys Compd.*, 2017, **695**, 818–826.
- 12 M. Downes, C. E. Shuck, B. McBride, J. Busa and Y. Gogotsi, *Nat. Protoc.*, 2024, **19**, 1807–1834.
- 13 S. Zhang, L. Meng, Y. Hu, Z. Yuan, J. Li and H. Liu, *Small*, 2024, **20**, 2308600.
- 14 S. Saxena, M. Johnson, F. Dixit, K. Zimmermann, S. Chaudhuri, F. Kaka and B. Kandasubramanian, *Renewable Sustainable Energy Rev.*, 2023, **178**, 113238.
- 15 P. Huang and W.-Q. Han, *Nano-Micro Lett.*, 2023, **15**, 68.
- 16 D. Gandla, Z. Zhuang, V. V. Jadhav and D. Q. Tan, *Energy Storage Mater.*, 2023, **63**, 102977.
- 17 M. A. Zaed, K. H. Tan, R. Saidur, N. Abdullah and A. K. Pandey, *J. Mater. Sci.*, 2024, **59**, 7575–7594.
- 18 S. Jolly, M. P. Paranthaman and M. Naguib, *Mater. Today Adv.*, 2021, **10**, 100139.
- 19 A. Rafieerad, A. Amiri, G. L. Sequiera, W. Yan, Y. Chen, A. A. Polycarpou and S. Dhingra, *Adv. Funct. Mater.*, 2021, **31**, 2100015.
- 20 S. M. M. Raj, A. K. Sundramoorthy, R. Atchudan, D. Ganapathy and A. Khosla, *J. Electrochem. Soc.*, 2022, **169**, 077501.
- 21 G. Cui, X. Zheng, X. Lv, Q. Jia, W. Xie and G. Gu, *Ceram. Int.*, 2019, **45**, 23600–23610.
- 22 S. Munir, A. Rasheed, T. Rasheed, I. Ayman, S. Ajmal, A. Rehman, I. Shakir, P. O. Agboola and M. F. Warsi, *ACS Omega*, 2020, **5**, 26845–26854.
- 23 L. Qu, Z. Zhao, Z. Li and R. Zhang, *Ceram. Int.*, 2024, **50**, 25115–25121.
- 24 M. Shen, W. Jiang, K. Liang, S. Zhao, R. Tang, L. Zhang and J.-Q. Wang, *Angew. Chem., Int. Ed.*, 2021, **60**, 27013–27018.
- 25 Z. Huang, X. Cui, S. Li, J. Wei, P. Li, Y. Wang and C.-S. Lee, *Nanophotonics*, 2020, **9**, 2233–2249.
- 26 M. Huang, Z. Gu, J. Zhang, D. Zhang, H. Zhang, Z. Yang and J. Qu, *J. Mater. Chem. B*, 2021, **9**, 5195–5220.
- 27 J. Huang, Z. Li, Y. Mao and Z. Li, *Nano Sel.*, 2021, **2**, 1480–1508.
- 28 S. Iravani and R. S. Varma, *Mater. Adv.*, 2021, **2**, 2906–2917.
- 29 A. Thakur, A. Pathania, A. Salvi, S. Kharbanda, N. Dhanda, M. Shandaliya, F. Wan and P. Thakur, *ChemBioEng Rev.*, 2023, **10**, 1050–1072.
- 30 M. Aslam, T. Ahmad, M. H. Manzoor and F. Verpoort, *Appl. Mater. Today*, 2023, **35**, 102002.
- 31 T. R. Dmytriv and V. I. Lushchak, *Chem. Rec.*, 2024, **24**, e202300338.
- 32 A. Szuplewska, D. Kulpińska, M. Jakubczak, A. Dybko, M. Chudy, A. Olszyna, Z. Brzózka and A. M. Jastrzębska, *Adv. Drug Delivery Rev.*, 2022, **182**, 114099.
- 33 H. Huang, R. Jiang, Y. Feng, H. Ouyang, N. Zhou, X. Zhang and Y. Wei, *Nanoscale*, 2020, **12**, 1325–1338.
- 34 J. B. Aswathanarayana, S. V. Madhunapantula and R. R. Vittal, *MXene Reinforced Polymer Composites*, John Wiley & Sons, Ltd, 2024, pp. 423–457.
- 35 S. M. George and B. Kandasubramanian, *Ceram. Int.*, 2020, **46**, 8522–8535.
- 36 M. Soleymaniha, M.-A. Shahbazi, A. R. Rafieerad, A. Maleki and A. Amiri, *Adv. Healthcare Mater.*, 2019, **8**, 1801137.
- 37 B. Xu, C. Zhi and P. Shi, *J. Phys. Mater.*, 2020, **3**, 031001.
- 38 M. R. Ali, M. S. Bacchu, M. R. Al-Mamun, M. I. Hossain, A. Khaleque, A. Khatun, D. D. Ridoy, M. A. S. Aly and



M. Z. H. Khan, *Crit. Rev. Anal. Chem.*, 2024, **54**, 1381–1398.

39 A. Parihar, A. Singhal, N. Kumar, R. Khan, M. A. Khan and A. K. Srivastava, *Nano-Micro Lett.*, 2022, **14**, 100.

40 D. Lu, H. Zhao, X. Zhang, Y. Chen and L. Feng, *Biosensors*, 2022, **12**, 820.

41 S. Iravani and R. S. Varma, *ACS Biomater. Sci. Eng.*, 2021, **7**, 1900–1913.

42 A. Sundaram, J. S. Ponraj, C. Wang, W. K. Peng, R. K. Manavalan, S. C. Dhanabalan, H. Zhang and J. Gaspar, *J. Mater. Chem. B*, 2020, **8**, 4990–5013.

43 K. Enoch, A. Sundaram, S. S. Ponraj, S. Palaniyappan, S. D. B. George and R. K. Manavalan, *Nanoscale*, 2023, **15**, 16874–16889.

44 J. Kim, A. S. Campbell, B. E.-F. de Ávila and J. Wang, *Nat. Biotechnol.*, 2019, **37**, 389–406.

45 Y. Yang, S. Yang, X. Xia, S. Hui, B. Wang, B. Zou, Y. Zhang, J. Sun and J. H. Xin, *ACS Nano*, 2024, **18**, 24705–24740.

46 R. Chen, X. Jia, H. Zhou, S. Ren, D. Han, S. Li and Z. Gao, *Mater. Today*, 2024, **75**, 359–385.

47 M. Ankitha, A. M. Arjun, N. Shabana and P. A. Rasheed, *Biomed. Mater. & Devices*, 2023, **1**, 339–350.

48 M. Xin, J. Li, Z. Ma, L. Pan and Y. Shi, *Front. Chem.*, 2020, **8**, 297.

49 M. Ankitha, F. Shamsheera and P. A. Rasheed, *ACS Appl. Electron. Mater.*, 2024, **6**, 599–610.

50 Y. Wang, Y. Yue, F. Cheng, Y. Cheng, B. Ge, N. Liu and Y. Gao, *ACS Nano*, 2022, **16**, 1734–1758.

51 Z. Luo, N. Kong, K. A. S. Usman, J. Tao, P. A. Lynch, J. M. Razal and J. Zhang, *Polymers*, 2024, **16**, 1824.

52 W. Pan, L. Xu, S. C. Lamont, Y. Zhang, J. Ding and F. J. Vernerey, *ACS Appl. Polym. Mater.*, 2024, **6**, 9488–9498.

53 H. Xia, L. Wang, H. Zhang, Z. Wang, L. Zhu, H. Cai, Y. Ma, Z. Yang and D. Zhang, *Microsyst. Nanoeng.*, 2023, **9**, 1–12.

54 S. Han, M. Zou, X. Pu, Y. Lu, Y. Tian, H. Li, Y. Liu, F. Wu, N. Huang, M. Shen, E. Song and D. Wang, *VIEW*, 2023, **4**, 20230005.

55 J. Wang, D. Zhang, D. Wang, Z. Xu, H. Zhang, X. Chen, Z. Wang, H. Xia and H. Cai, *ACS Appl. Mater. Interfaces*, 2023, **15**, 37946–37956.

56 Y. Su, K. Ma, M. Liu and X. Zhang, *Phys. Scr.*, 2023, **98**, 035032.

57 L. Liu, T. Luo, X. Kuang, X. Wan, X. Liang, G. Jiang, H. Cong and H. He, *ACS Sens.*, 2024, **9**, 2476–2487.

58 C. Jin and Z. Bai, *ACS Sens.*, 2022, **7**, 929–950.

59 Q. Yu, C. Su, S. Bi, Y. Huang, J. Li, H. Shao, J. Jiang and N. Chen, *ACS Appl. Mater. Interfaces*, 2022, **14**, 9632–9643.

60 Y. Zheng, R. Yin, Y. Zhao, H. Liu, D. Zhang, X. Shi, B. Zhang, C. Liu and C. Shen, *Chem. Eng. J.*, 2021, **420**, 127720.

61 S. Wang, X. Du, Y. Luo, S. Lin, M. Zhou, Z. Du, X. Cheng and H. Wang, *Chem. Eng. J.*, 2021, **408**, 127363.

62 Y. Sun, S. Wang, X. Du, Z. Du, H. Wang and X. Cheng, *J. Mater. Chem. B*, 2021, **9**, 8667–8675.

63 M. Chao, P. Di, Y. Yuan, Y. Xu, L. Zhang and P. Wan, *Nano Energy*, 2023, **108**, 108201.

64 M. Chao, L. He, M. Gong, N. Li, X. Li, L. Peng, F. Shi, L. Zhang and P. Wan, *ACS Nano*, 2021, **15**, 9746–9758.

65 L. Yang, H. Wang, W. Yuan, Y. Li, P. Gao, N. Tiwari, X. Chen, Z. Wang, G. Niu and H. Cheng, *ACS Appl. Mater. Interfaces*, 2021, **13**, 60531–60543.

66 M. Chao, Y. Wang, D. Ma, X. Wu, W. Zhang, L. Zhang and P. Wan, *Nano Energy*, 2020, **78**, 105187.

67 K. Zhang, J. Sun, J. Song, C. Gao, Z. Wang, C. Song, Y. Wu and Y. Liu, *ACS Appl. Mater. Interfaces*, 2020, **12**, 45306–45314.

68 J. Xu, L. Zhang, X. Lai, X. Zeng and H. Li, *ACS Appl. Mater. Interfaces*, 2022, **14**, 27262–27273.

69 Y. Liu, G. Tian, Y. Du, P. Shi, N. Li, Y. Li, Z. Qin, T. Jiao and X. He, *Adv. Funct. Mater.*, 2024, **34**, 2315813.

70 P. K. Kalambate, N. S. Gadhari, X. Li, Z. Rao, S. T. Navale, Y. Shen, V. R. Patil and Y. Huang, *TrAC, Trends Anal. Chem.*, 2019, **120**, 115643.

71 F. Shahzad, S. A. Zaidi and R. A. Naqvi, *Crit. Rev. Anal. Chem.*, 2022, **52**, 848–864.

72 S. Ali, P. M. Ismail, M. Bououdina and G. Yasin, in *Mxene-Based Hybrid Nano-Architectures for Environmental Remediation and Sensor Applications*, ed. R. K. Gupta, M. Bilal, T. A. Nguyen, H. M. N. Iqbal and G. Yasin, Elsevier, 2024, pp. 417–450.

73 G. Ji, J. Wang, Z. Wang, S. Zhang, Z. Fang, Y. Wang and Z. Gao, *Biosens. Bioelectron.*, 2024, **261**, 116509.

74 F. Chen, J. Wang, L. Chen, H. Lin, D. Han, Y. Bao, W. Wang and L. Niu, *Anal. Chem.*, 2024, **96**, 3914–3924.

75 Y. Pan, M. He, J. Wu, H. Qi and Y. Cheng, *Sens. Actuators, B*, 2024, **401**, 135055.

76 Y. Lei, W. Zhao, Y. Zhang, Q. Jiang, J.-H. He, A. J. Baeumner, O. S. Wolfbeis, Z. L. Wang, K. N. Salama and H. N. Alshareef, *Small*, 2019, **15**, 1901190.

77 S. Kalasin and P. Sangnuang, *ACS Appl. Nano Mater.*, 2023, **6**, 18209–18221.

78 T. J. Mun, E. Yang, J. Moon, S. Kim, S. G. Park, M. Kim, N. Choi, Y. Lee, S. J. Kim and H. Seong, *ACS Appl. Polym. Mater.*, 2024, **6**, 9533–9544.

79 M. A. Zahed, M. Sharifuzzaman, H. Yoon, M. Asaduzzaman, D. K. Kim, S. Jeong, G. B. Pradhan, Y. D. Shin, S. H. Yoon, S. Sharma, S. Zhang and J. Y. Park, *Adv. Funct. Mater.*, 2022, **32**, 2208344.

80 S. Singh, A. Numan, M. Khalid, I. Bello, E. Panza and S. Cinti, *Small*, 2023, **19**, 2208209.

81 W. Alfalasi, T. Hussain and N. Tit, *Sci. Rep.*, 2024, **14**, 1403.

82 Y. Zhang, Z. Wang, X. Liu, Y. Liu, Y. Cheng, D. Cui, F. Chen and W. Cao, *FlatChem*, 2023, **39**, 100503.

83 J. Zhao, C. He, W. Wu, H. Yang, L. Peng, L. Wen, Z. Hu, C. Hou and D. Huo, *Chem. Eng. J.*, 2022, **446**, 136841.

84 S. Boobphahom, T. Siripongpreda, D. Zhang, J. Qin, P. Rattanawaleedirojn and N. Rodthongkum, *Microchim. Acta*, 2021, **188**, 387.

85 Q.-F. Li, X. Chen, H. Wang, M. Liu and H.-L. Peng, *ACS Appl. Mater. Interfaces*, 2023, **15**, 13290–13298.



86 V. Myndrul, E. Coy, N. Babayevska, V. Zahorodna, V. Balitskyi, I. Baginskiy, O. Gogotsi, M. Bechelany, M. T. Giardi and I. Iatsunskyi, *Biosens. Bioelectron.*, 2022, **207**, 114141.

87 J. S. Nah, S. C. Barman, M. A. Zahed, M. Sharifuzzaman, H. Yoon, C. Park, S. Yoon, S. Zhang and J. Y. Park, *Sens. Actuators, B*, 2021, **329**, 129206.

88 A. Zamhuri, G. P. Lim, N. L. Ma, K. S. Tee and C. F. Soon, *Biomed. Eng. Online*, 2021, **20**, 33.

89 A. M. Amani, E. Vafa, M. Mirzae, M. Abbasi, A. Vaez, A. Najdian, A. Jahanbin, S. R. Kasaei, S. Mosleh-Shirazi, H. Kamyab, S. Chelliapan, S. Rajendran and L. P. Guamán, *J. Ind. Eng. Chem.*, 2025, DOI: [10.1016/j.jiec.2025.02.020](https://doi.org/10.1016/j.jiec.2025.02.020).

90 C. Dai, Y. Chen, X. Jing, L. Xiang, D. Yang, H. Lin, Z. Liu, X. Han and R. Wu, *ACS Nano*, 2017, **11**, 12696–12712.

91 Z. Liu, H. Lin, M. Zhao, C. Dai, S. Zhang, W. Peng and Y. Chen, *Theranostics*, 2018, **8**, 1648–1664.

92 L. Zong, H. Wu, H. Lin and Y. Chen, *Nano Res.*, 2018, **11**, 4149–4168.

93 Y. Wu, W. Xiong, Z. Wang, Y. Wang, K. Sun, X. Song, Z. Lv, W. Xu, W. Zhong, X. Zou, H.-L. Cai and X. Wu, *Chem. Eng. J.*, 2022, **427**, 131925.

94 T. Wang, W. Gu, L. Yu, X. Guo, J. Yang, X. Sun, J. Guan, L. Zhou, C. Wang, H. Yao, X. Zhang and G. Wang, *J. Materomics*, 2023, **9**, 1129–1140.

95 V. Neubertova, O. Guselnikova, Y. Yamauchi, A. Olshtrem, S. Rimpelova, E. Čižmár, M. Orendáč, J. Duchon, L. Volfova, J. Lancok, V. Herynek, P. Fitl, P. Ulbrich, L. Jelinek, P. Schneider, J. Kosek, P. Postnikov, Z. Kolska, V. Svorcik, S. Chertopalov and O. Lyutakov, *Chem. Eng. J.*, 2022, **446**, 136939.

96 B. Gürbüz and F. Ciftci, *Chem. Eng. J.*, 2024, **489**, 151230.

97 S. Iravani, E. Nazarzadeh Zare and P. Makvandi, *ACS Biomater. Sci. Eng.*, 2024, **10**, 1892–1909.

98 P. Abdollahiyan, F. Oroojalian, M. Hejazi, M. de la Guardia and A. Mokhtarzadeh, *J. Controlled Release*, 2021, **333**, 391–417.

99 K. Zhang, S. Wang, C. Zhou, L. Cheng, X. Gao, X. Xie, J. Sun, H. Wang, M. D. Weir, M. A. Reynolds, N. Zhang, Y. Bai and H. H. K. Xu, *Bone Res.*, 2018, **6**, 1–15.

100 X. Zhang, C. Zhang, Y. Lin, P. Hu, Y. Shen, K. Wang, S. Meng, Y. Chai, X. Dai, X. Liu, Y. Liu, X. Mo, C. Cao, S. Li, X. Deng and L. Chen, *ACS Nano*, 2016, **10**, 7279–7286.

101 J. Zhang, Y. Fu and A. Mo, *Int. J. Nanomed.*, 2019, **14**, 10091–10103.

102 X. Mi, Z. Su, Y. Fu, S. Li and A. Mo, *Biomed. Mater.*, 2022, **17**, 035002.

103 R. Nie, Y. Sun, H. Lv, M. Lu, H. Huangfu, Y. Li, Y. Zhang, D. Wang, L. Wang and Y. Zhou, *Nanoscale*, 2022, **14**, 8112–8129.

104 S. Pan, J. Yin, L. Yu, C. Zhang, Y. Zhu, Y. Gao and Y. Chen, *Adv. Sci.*, 2020, **7**, 1901511.

105 J. Yin, S. Pan, X. Guo, Y. Gao, D. Zhu, Q. Yang, J. Gao, C. Zhang and Y. Chen, *Nano-Micro Lett.*, 2021, **13**, 30.

106 Z.-C. Hu, J.-Q. Lu, T.-W. Zhang, H.-F. Liang, H. Yuan, D.-H. Su, W. Ding, R.-X. Lian, Y.-X. Ge, B. Liang, J. Dong, X.-G. Zhou and L.-B. Jiang, *Bioact. Mater.*, 2023, **22**, 1–17.

107 Y. Hu, Z. Xu, J. Pu, L. Hu, Y. Zi, M. Wang, X. Feng and W. Huang, *Front. Chem.*, 2022, **10**, 1090905.

108 K. Chen, Y. Chen, Q. Deng, S.-H. Jeong, T.-S. Jang, S. Du, H.-E. Kim, Q. Huang and C.-M. Han, *Mater. Lett.*, 2018, **229**, 114–117.

109 Z. Xu, Y. Zhang, H. Dai, Y. Wang, Y. Ma, S. Tan and B. Han, *J. Ind. Eng. Chem.*, 2022, **114**, 536–548.

110 C. K. Balavigneswaran and V. Muthuvijayan, in *Biomaterials in Tissue Engineering and Regenerative Medicine: From Basic Concepts to State of the Art Approaches*, ed. B. Bhaskar, P. Sreenivasa Rao, N. Kasaju, V. Nagarjuna and R. R. Baadhe, Springer, Singapore, 2021, pp. 381–422.

111 A. Rozmysłowska-Wojciechowska, J. Mitrzak, A. Szuplewska, M. Chudy, J. Woźniak, M. Petrus, T. Wojciechowski, A. S. Vasilchenko and A. M. Jastrzębska, *Materials*, 2020, **13**, 2347.

112 J. Ye, C. Xie, C. Wang, J. Huang, Z. Yin, B. C. Heng, X. Chen and W. Shen, *Bioact. Mater.*, 2021, **6**, 4096–4109.

113 H. Hashimoto, E. N. Olson and R. Bassel-Duby, *Nat. Rev. Cardiol.*, 2018, **15**, 585–600.

114 M. Liao, Q. Cui, Y. Hu, J. Xing, D. Wu, S. Zheng, Y. Zhao, Y. Yu, J. Sun and R. Chai, *Neural. Regen. Res.*, 2023, **19**, 258–263.

115 B. Luo, X. Bai, Y. Hou, J. Guo, Z. Liu, Y. Duan and Z. Wu, *Int. J. Biol. Macromol.*, 2025, **303**, 140613.

116 A. Zarepour, N. Rafati, A. Khosravi, N. Rabiee, S. Iravani and A. Zarrabi, *Nanoscale Adv.*, 2024, **6**, 3513–3532.

117 L. Chen, X. Dai, W. Feng and Y. Chen, *Acc. Mater. Res.*, 2022, **3**, 785–798.

118 G. P. Lim, C. F. Soon, N. L. Ma, M. Morsin, N. Nayan, M. K. Ahmad and K. S. Tee, *Environ. Res.*, 2021, **201**, 111592.

119 A. M. Amani, A. Rahbar, E. Vafa, L. Tayebi, M. Abbasi, H. Kamyab, S. Chelliapan, S. R. Kasaei, A. Vaez and S. Mosleh-Shirazi, *Mater. Today Commun.*, 2024, **41**, 110774.

120 V. Ferrara, C. Perfili, G. Artemi, B. Iacolino, F. Sciandra, G. Perini, L. Fusco, M. Pogorielov, L. G. Delogu, M. Papi, M. D. Spirito and V. Palmieri, *Nanoscale*, 2024, **16**, 18684–18714.

121 G. A. Asaro, M. Solazzo, M. Suku, D. Spurling, K. Genoud, J. G. Gonzalez, F. J. O. Brien, V. Nicolosi and M. G. Monaghan, *npj 2D Mater. Appl.*, 2023, **7**, 1–13.

122 L. P. Nan, Z. Lin, F. Wang, X. H. Jin, J. Q. Fang, B. Xu, S. H. Liu, F. Zhang, Z. Wu, Z. F. Zhou and F. Chen, *Front. Bioeng. Biotechnol.*, 2022, **10**, 850650.

123 Y. Wang, R. Garg, J. E. Hartung, A. Goad, D. A. Patel, F. Vitale, M. S. Gold, Y. Gogotsi and T. Cohen-Karni, *ACS Nano*, 2021, **15**, 14662–14671.

124 R. Guo, M. Xiao, W. Zhao, S. Zhou, Y. Hu, M. Liao, S. Wang, X. Yang, R. Chai and M. Tang, *Acta Biomater.*, 2022, **139**, 105–117.



125 Q. Yu, S. Jin, S. Wang, H. Xiao and Y. Zhao, *Chem. Eng. J.*, 2023, **452**, 139252.

126 J. Cai, H. Zhang, Y. Hu, Z. Huang, Y. Wang, Y. Xia, X. Chen, J. Guo, H. Cheng, L. Xia, W. Lu, C. Zhang, J. Xie, H. Wang and R. Chai, *J. Nanobiotechnol.*, 2022, **20**, 460.

127 Z. Wang, Y. Zheng, L. Qiao, Y. Ma, H. Zeng, J. Liang, Q. Ye, K. Shen, B. Liu, L. Sun and Z. Fan, *Adv. Healthcare Mater.*, 2024, **13**, 2401093.

128 K. N. Alagarsamy, S. Mathan, W. Yan, A. Rafieerad, S. Sekaran, H. Manego and S. Dhingra, *Bioact. Mater.*, 2021, **6**, 2261–2280.

129 K. Ashtari, H. Nazari, H. Ko, P. Tebon, M. Akhshik, M. Akbari, S. N. Alhosseini, M. Mozafari, B. Mehravi, M. Soleimani, R. Ardehali, M. E. Warkiani, S. Ahadian and A. Khademhosseini, *Adv. Drug Delivery Rev.*, 2019, **144**, 162–179.

130 M. Yadid, R. Feiner and T. Dvir, *Nano Lett.*, 2019, **19**, 2198–2206.

131 K. Diedkova, A. D. Pogrebnyak, S. Kyrylenko, K. Smyrnova, V. V. Buranich, P. Horodek, P. Zukowski, T. N. Koltunowicz, P. Galaszkiewicz, K. Makashina, V. Bondariev, M. Sahul, M. Čaplovičová, Y. Husak, W. Simka, V. Korniienko, A. Stolarczyk, A. Blacha-Grzechnik, V. Balitskyi, V. Zahorodna, I. Baginskiy, U. Riekstina, O. Gogotsi, Y. Gogotsi and M. Pogorielov, *ACS Appl. Mater. Interfaces*, 2023, **15**, 14033–14047.

132 K. Diedkova, Y. Husak, W. Simka, V. Korniienko, B. Petrovic, A. Roshchupkin, A. Stolarczyk, N. Waloszczyk, I. Yanko, K. Jekabsons, M. Čaplovičová, A. D. Pogrebnyak, V. Zahorodna, O. Gogotsi, I. Roslyk, I. Baginskiy, M. Radovic, S. Kojic, U. Riekstina and M. Pogorielov, *Graphene 2D Mater.*, 2024, **9**, 59–76.

133 M. Lee, J. Park, G. Choe, S. Lee, B. G. Kang, J. H. Jun, Y. Shin, M. C. Kim, Y. S. Kim, Y. Ahn and J. Y. Lee, *ACS Nano*, 2023, **17**, 12290–12304.

134 R. E. Ahmed, T. Anzai, N. Chanthra and H. Uosaki, *Front. Cell Dev. Biol.*, 2020, **8**, 178.

135 G. Basara, M. Saeidi-Javash, X. Ren, G. Bahcecioglu, B. C. Wyatt, B. Anasori, Y. Zhang and P. Zorlutuna, *Acta Biomater.*, 2022, **139**, 179–189.

136 A. Rafieerad, W. Yan, G. L. Sequiera, N. Sareen, E. Abu-El-Rub, M. Moudgil and S. Dhingra, *Adv. Healthcare Mater.*, 2019, **8**, 1900569.

137 B. Song, Y. Gu, J. Pu, B. Reid, Z. Zhao and M. Zhao, *Nat. Protoc.*, 2007, **2**, 1479–1489.

138 Y. Long, H. Wei, J. Li, G. Yao, B. Yu, D. Ni, A. L. Gibson, X. Lan, Y. Jiang, W. Cai and X. Wang, *ACS Nano*, 2018, **12**, 12533–12540.

139 R. Yu, H. Zhang and B. Guo, *Nano-Micro Lett.*, 2021, **14**, 1.

140 L. Mao, S. Hu, Y. Gao, L. Wang, W. Zhao, L. Fu, H. Cheng, L. Xia, S. Xie, W. Ye, Z. Shi and G. Yang, *Adv. Healthcare Mater.*, 2020, **9**, 2000872.

141 H. Park, J.-U. Kim, S. Kim, N. S. Hwang and H. D. Kim, *Mater. Today Bio*, 2023, **23**, 100881.

142 X. Yang, C. Zhang, D. Deng, Y. Gu, H. Wang and Q. Zhong, *Small*, 2022, **18**, 2104368.

143 Y. Yang, X. Zhou, Y. K. Chan, Z. Wang, L. Li, J. Li, K. Liang and Y. Deng, *Small*, 2022, **18**, 2105988.

144 M. Liu, L. Zheng, K. Zha, Y. Yang, Y. Hu, K. Chen, F. Wang, K. Zhang, W. Liu, B. Mi, X. Xiao and Q. Feng, *Front. Bioeng. Biotechnol.*, 2023, **11**, 1308184.

145 C. Liang, H. Wang, Z. Lin, C. Zhang, G. Liu and Y. Hu, *Front. Bioeng. Biotechnol.*, 2023, **11**, 1310349.

146 L. Jin, X. Guo, D. Gao, Y. Liu, J. Ni, Z. Zhang, Y. Huang, G. Xu, Z. Yang, X. Zhang and X. Jiang, *Bioact. Mater.*, 2022, **16**, 162–172.

147 H. Li, M. Mu, B. Chen, L. Zhou, B. Han and G. Guo, *Mater. Res. Lett.*, 2024, **12**, 67–87.

148 Z. Wu, S. Li, X. Qin, L. Zheng, J. Fang, L. Wei, C. Xu, Z. A. Li and X. Wang, *Carbohydr. Polym.*, 2024, **334**, 121934.

149 X. Ju, J. Kong, G. Qi, S. Hou, B. Wang, X. Diao, S. Dong and Y. Jin, *eScience*, 2024, **4**, 100223.

150 B. Li, W. Yang, R. Shu, H. Yang, F. Yang, W. Dai, W. Chen, Y. K. Chan, D. Bai and Y. Deng, *Adv. Mater.*, 2024, **36**, 2307613.

151 G. Cooksley, M. K. Dymond, N. A. Stewart, G. Bucca, A. Hesketh, J. Lacey, Y. Gogotsi and S. Sandeman, *2D Mater.*, 2022, **10**, 014003.

152 L. Chen, H. Deng, H. Cui, J. Fang, Z. Zuo, J. Deng, Y. Li, X. Wang and L. Zhao, *Oncotarget*, 2017, **9**, 7204–7218.

153 Y. Huang, X. Guo, Y. Wu, X. Chen, L. Feng, N. Xie and G. Shen, *Signal Transduct. Target. Ther.*, 2024, **9**, 1–50.

154 E. Tobin and S. Brenner, *Open Forum Infect. Dis.*, 2021, **8**, ofab583.

155 L. Singh, H. G. Kruger, G. E. M. Maguire, T. Govender and R. Parboosing, *Ther. Adv. Infect. Dis.*, 2017, **4**, 105–131.

156 K. N. Sharma, J. Yadav, S. Singh, H. Joshi and K. Behera, *MXenes as Surface-Active Advanced Materials*, Elsevier, 2024, pp. 501–523.

157 S. Lu, G. Meng, C. Wang and H. Chen, *Chem. Eng. J.*, 2021, **404**, 126526.

158 X. Zhu, Y. Zhu, K. Jia, B. S. Abraha, Y. Li, W. Peng, F. Zhang, X. Fan and L. Zhang, *Nanoscale*, 2020, **12**, 19129–19141.

159 K. Rajavel, S. Shen, T. Ke and D. Lin, *Appl. Surf. Sci.*, 2021, **538**, 148083.

160 A. Arabi Shamsabadi, M. Sharifian Gh, B. Anasori and M. Soroush, *ACS Sustainable Chem. Eng.*, 2018, **6**, 16586–16596.

161 E. A. Mayerberger, R. M. Street, R. M. McDaniel, M. W. Barsoum and C. L. Schauer, *RSC Adv.*, 2018, **8**, 35386–35394.

162 K. Rasool, K. A. Mahmoud, D. J. Johnson, M. Helal, G. R. Berdiyorov and Y. Gogotsi, *Sci. Rep.*, 2017, **7**, 1598.

163 R. P. Pandey, P. A. Rasheed, T. Gomez, K. Rasool, J. Ponraj, K. Prenger, M. Naguib and K. A. Mahmoud, *ACS Appl. Nano Mater.*, 2020, **3**, 11372–11382.

164 G. Zamiri, A. A. Babadi, V. Chaudhary, A. Numan, M. Khalid, R. Walvekar and A. Khosla, *J. Electrochem. Soc.*, 2023, **170**, 037501.



165 R. Srivastava, S. Pal and Y. K. Prajapati, *Plasmonics*, 2023, **18**, 2049–2058.

166 W. Li, X. Bai, F. Xiao, J. Huang, X. Zeng, Q. Xu, Y. Song, X. Xu and H. Xu, *J. Hazard. Mater.*, 2023, **457**, 131823.

167 G. Park, M. Lee, J. Kang, C. Park, J. Min and T. Lee, *Nano Convergence*, 2022, **9**, 41.

168 A. Bharti, S. Singh, D. Munthala, S. Roy, S. Pojprapai, S. Suksaweang, S. Sain, S. S. Roy, J. J. Mohamed, D. K. Avasthi and A. Mathur, *Microchem. J.*, 2023, **195**, 109521.

169 M. A. Unal, F. Bayrakdar, L. Fusco, O. Besbinar, C. E. Shuck, S. Yalcin, M. T. Erken, A. Ozkul, C. Gurcan, O. Panatli, G. Y. Summak, C. Gokce, M. Orecchioni, A. Gazzi, F. Vitale, J. Somers, E. Demir, S. S. Yildiz, H. Nazir, J.-C. Grivel, D. Bedognetti, A. Crisanti, K. C. Akcali, Y. Gogotsi, L. G. Delogu and A. Yilmazer, *Nano Today*, 2021, **38**, 101136.

170 W. Y. Chen, H. Lin, A. K. Barui, A. M. U. Gomez, M. K. Wendt and L. A. Stanciu, *ACS Appl. Nano Mater.*, 2022, **5**, 1902–1910.

171 X. Peng, Y. Zhang, D. Lu, Y. Guo and S. Guo, *Sens. Actuators, B*, 2019, **286**, 222–229.

172 Y. Wang, W. Sun, Y. Li, X. Zhuang, C. Tian, F. Luan and X. Fu, *Microchem. J.*, 2021, **167**, 106332.

173 H. A. Nguyen, N. T. T. Phuong, T. N. D. Trinh, N. H. T. Tran and K. T. L. Trinh, *Sens. Actuators, A*, 2024, **378**, 115784.

174 R. Chen, L. Kan, F. Duan, L. He, M. Wang, J. Cui, Z. Zhang and Z. Zhang, *Microchim. Acta*, 2021, **188**, 316.

175 Q. Wu, W. Wu, F. Chen and P. Ren, *Analyst*, 2022, **147**, 2809–2818.

176 W. Yang, R. Liu, J. Yan, Y. Xie, C. Wang, M. Jiang, P. Li and L. Du, *Biosens. Bioelectron.*, 2023, **235**, 115358.

177 Y. Peng, C. Lin, L. Long, T. Masaki, M. Tang, L. Yang, J. Liu, Z. Huang, Z. Li, X. Luo, J. R. Lombardi and Y. Yang, *Nano-Micro Lett.*, 2021, **13**, 52.

178 C. Wang, J. Han, D. Xue, C. Gu, S. Zeng, J. Jiang, T. Jiang, X. Li and K. Wu, *Spectrochim. Acta, Part A*, 2024, **305**, 123445.

179 N. Dwivedi, C. Dhand, P. Kumar and A. K. Srivastava, *Mater. Adv.*, 2021, **2**, 2892–2905.

180 X. Zhao, Y. Chen, R. Niu, Y. Tang, Y. Chen, H. Su, Z. Yang, X. Jing, H. Guan, R. Gao and L. Meng, *Adv. Mater.*, 2024, **36**, 2307839.

181 J. Liu, Z. Liu, Y. Pang and H. Zhou, *J. Nanobiotechnol.*, 2022, **20**, 127.

182 R. Soltani, S. Guo, A. Bianco and C. Ménard-Moyon, *Adv. Ther.*, 2020, **3**, 2000051.

183 J. Deng, D. Xian, X. Cai, S. Liao, S. Lei, F. Han, Y. An, Q. He, G. Quan, C. Wu, T. Peng, C. Lu and H. Zhang, *Adv. Funct. Mater.*, 2023, **33**, 2211846.

184 C. He, L. Yu, H. Yao, Y. Chen and Y. Hao, *Adv. Funct. Mater.*, 2021, **31**, 2006214.

185 Y. Li, R. Fu, Z. Duan, C. Zhu and D. Fan, *ACS Nano*, 2022, **16**, 7486–7502.

186 G. Ye, Z. Wen, F. Wen, X. Song, L. Wang, C. Li, Y. He, S. Prakash and X. Qiu, *Theranostics*, 2020, **10**, 2047–2066.

187 J. Zhang, Y. Wang, N. Ding, P. Ma, Z. Zhang and Y. Liu, *Colloid Interface Sci. Commun.*, 2023, **56**, 100733.

188 B. Sha, S. Zhao, M. Gu, D. Khodagholy, L. Wang, G. Q. Bi and Z. Du, *Proc. Natl. Acad. Sci. U. S. A.*, 2023, **120**, e2306777120.

189 L. Hou, F. Gong, B. Liu, X. Yang, L. Chen, G. Li, Y. Gong, C. Liang, N. Yang, X. Shen, Z. Liu and L. Cheng, *Theranostics*, 2022, **12**, 3834–3846.

190 Y. Huang, S. He, S. Yu, H. M. Johnson, Y. K. Chan, Z. Jiao, S. Wang, Z. Wu and Y. Deng, *Small*, 2024, **20**, 2304119.

191 W. Yan, A. Rafieerad, K. N. Alagarsamy, L. R. Saleth, R. C. Arora and S. Dhingra, *Nano Today*, 2023, **48**, 101706.

192 A. Rafieerad, W. Yan, K. N. Alagarsamy, A. Srivastava, N. Sareen, R. C. Arora and S. Dhingra, *Adv. Funct. Mater.*, 2021, **31**, 2106786.

193 A. Yilmazer, K. N. Alagarsamy, C. Gokce, G. Y. Summak, A. Rafieerad, F. Bayrakdar, B. I. Ozturk, S. Aktuna, L. G. Delogu, M. A. Unal and S. Dhingra, *Small Methods*, 2023, **7**, 2300044.

194 T. A. Oyehan, B. A. Salami, A. A. Abdulrasheed, H. U. Hambali, A. Gbadamosi, E. Valsami-Jones and T. A. Saleh, *Appl. Mater. Today*, 2023, **35**, 101993.

195 I. A. Vasyukova, O. V. Zakharova, D. V. Kuznetsov and A. A. Gusev, *Nanomaterials*, 2022, **12**, 1797.

196 J. Wu, Y. Yu and G. Su, *Nanomaterials*, 2022, **12**, 828.

197 D. Parajuli, *Front. Chem.*, 2024, **12**, 1400375.

198 S. Kulkarni, S. Soman, P. D. Navti, A. A. Roy, A. N. Nikam, P. Vineeth, J. Kulkarni, K. S. Shirur, A. Pandey, S. D. George and S. Mutualik, *Materials*, 2024, **17**, 1423.

199 S. Soman, S. Kulkarni, A. Pandey, N. Dhas, K. S. Shirur, R. S. Gude, S. M. Vidya, S. Nayak, S. D. George and S. Mutualik, *Mater. Today Commun.*, 2024, **38**, 107711.

